J. Fluid Mech. (1991), *vol.* 228, *pp.* 149–181
Printed in Great Britain

On the stability of vertical double-diffusive interfaces. Part 1. A single plane interface

By I. A. ELTAYEB[1] AND D. E. LOPER[2]

[1] Department of Mathematics and Computing, Sultan Qaboos University, Muscat, Sultanate of Oman

[2] Department of Mathematics, Florida State University, Tallahassee, FL 32306, USA

(Received 25 August 1989 and in revised form 19 December 1990)

This is the first part of a three-part study of the stability of vertically oriented double-diffusive interfaces having an imposed vertical stable temperature gradient. Flow is forced by a prescribed jump of composition across the interfaces. Compositional diffusivity is ignored, while thermal diffusivity and viscosity are finite. In this first part, basic-state solutions are presented and discussed for three configurations: a single plane interface, two parallel interfaces and a circular cylindrical interface.

The stability of a single plane interface is then analysed. It is shown that the presence of the compositional jump gives rise to a new type of three-dimensional instability which occurs for any non-zero forcing. This is in contrast to the thermally driven flow adjacent to a rigid wall, which is unstable only for a finite value of the forcing and results in the growth of a two-dimensional perturbation. The timescale for growth of the new instability is given by

$$\tau = \left[\frac{\nu\rho}{(\Delta\rho)_C}\right]^2 \frac{\alpha}{\kappa g}\frac{\mathrm{d}T}{\mathrm{d}z},$$

where $(\Delta\rho)_C$ is the prescribed jump in composition and $\mathrm{d}T/\mathrm{d}z$ is the imposed temperature gradient.

The influence of thermal diffusion is to enhance instability, while viscosity is stabilizing for nearly all wavenumbers. The interface is unstable for all finite wavenumbers if the Prandtl number is less than 1.472, while regions of stability in the wavenumber plane develop for small horizontal wavenumber and moderate vertical wavenumber for larger values of the Prandtl number. The neutral stability curves are investigated and the maximum growth rate of instability is identified for the whole range of values of the Prandtl number and its properties are elucidated by comparison with previous studies of flows near heated vertical walls.

1. Introduction

Double-diffusive convective flows occur in a wide variety of situations (Huppert & Moore 1976; Chen & Johnson 1984; Turner 1985) and this variety has motivated studies of the behaviour of nearly all possible configurations of imposed compositional and thermal gradients. Most studies have concentrated on horizontal interfaces across which vertical gradients of temperature and composition are imposed, with relative little attention being paid to vertical interfaces. This paper is the first of a three-part study of the stability of vertical interfaces, across which are imposed

jumps in composition and temperature, in the presence of a vertically oriented stabilizing temperature gradient.

Three simple geometries are to be considered: a single plane interface, two parallel interfaces (i.e. a Cartesian plume) and a circular cylindrical interface (i.e. a cylindrical plume). In each case the composition and temperature prescribed on either side of the interfaces are such that there is no jump in density; in the absence of diffusive effects, the system is static and stable. The compositional diffusivity is assumed to be zero and the compositional interfaces sharp, while viscosity and thermal diffusivity are finite so that temperature and velocity vary smoothly.

With the chosen orientation of thermal and compositional gradients and finite thermal diffusivity, a hydrostatic state is not possible. Thermal diffusion alters the density of the fluid close to the interfaces, which induces vertical flow, analogous to a catabatic wind. This flow and the associated thermal field are referred to as the basic state. For each of the chosen geometries analytic basic-state solutions, dependent on a single horizontal coordinate, have been found.

We wish to determine the stability of the shape of these interfaces, in the presence of these basic-state flows, to infinitesimal harmonic perturbations. The stability of a single plane interface is considered here in Part 1, while the stability of the other two configurations will be detailed in future papers (Parts 2 and 3).

The present investigation was motivated by a desire to understand the instability of compositionally buoyant plumes rising through a homogeneous, thermally stably stratified fluid, as described by Copley *et al.* (1970). These plumes, which have a circular horizontal cross-section, exhibit a helical instability; see figure 1. We wish to gain an understanding and accurate description of this instability. This knowledge may be of use in prescribing the flow field within the Earth's core which sustains the geomagnetic field by dynamo action (Loper 1989).

The geometrically simpler and analytically tractable cases of a single and double plane interface will be studied first to gain insight into the behaviour of the system before analysing the cylindrical case numerically. The present study of the stability of a single plane interface may also have application to the behaviour of oceanographic fronts, although such fronts usually occur on a much larger scale than those considered here and result from different dynamic balances (Hsueh & Cushman-Roisin 1983; Ou 1983; Wang 1984; Chapman 1986).

The problem of the stability of the single plane interface studied here shows some similarity with the problem posed by a heated rigid vertical wall studied by Gill & Davey (1969) and Dudis & Davis (1971). However, the two problems are different because of the differing natures of the boundary at the 'wall' at $x = 0$. The rigid wall imposes the conditions that the perturbations in velocity and temperature must *vanish* at $x = 0$, whereas for the present problem a free boundary at $x = 0$ requires the *continuity* of velocity, temperature, stress and heat flux. This difference of conditions has two implications. First the instabilities isolated for the rigid-wall problem are modified by the change to free-boundary conditions. Second, and more important, is the appearance of a *new* type of instability coupled to the deformation of the interface. For the free-boundary problem studied here, this new instability is preferred at small values of the forcing. We shall therefore restrict the study below to this new instability.

Studies of the heated-wall problem have been confined to two-dimensional perturbations, i.e. perturbations which depend on the vertical coordinate and the horizontal coordinate normal to the wall, while the analysis below deals with both two- and three-dimensional perturbations. This is particularly relevant since the

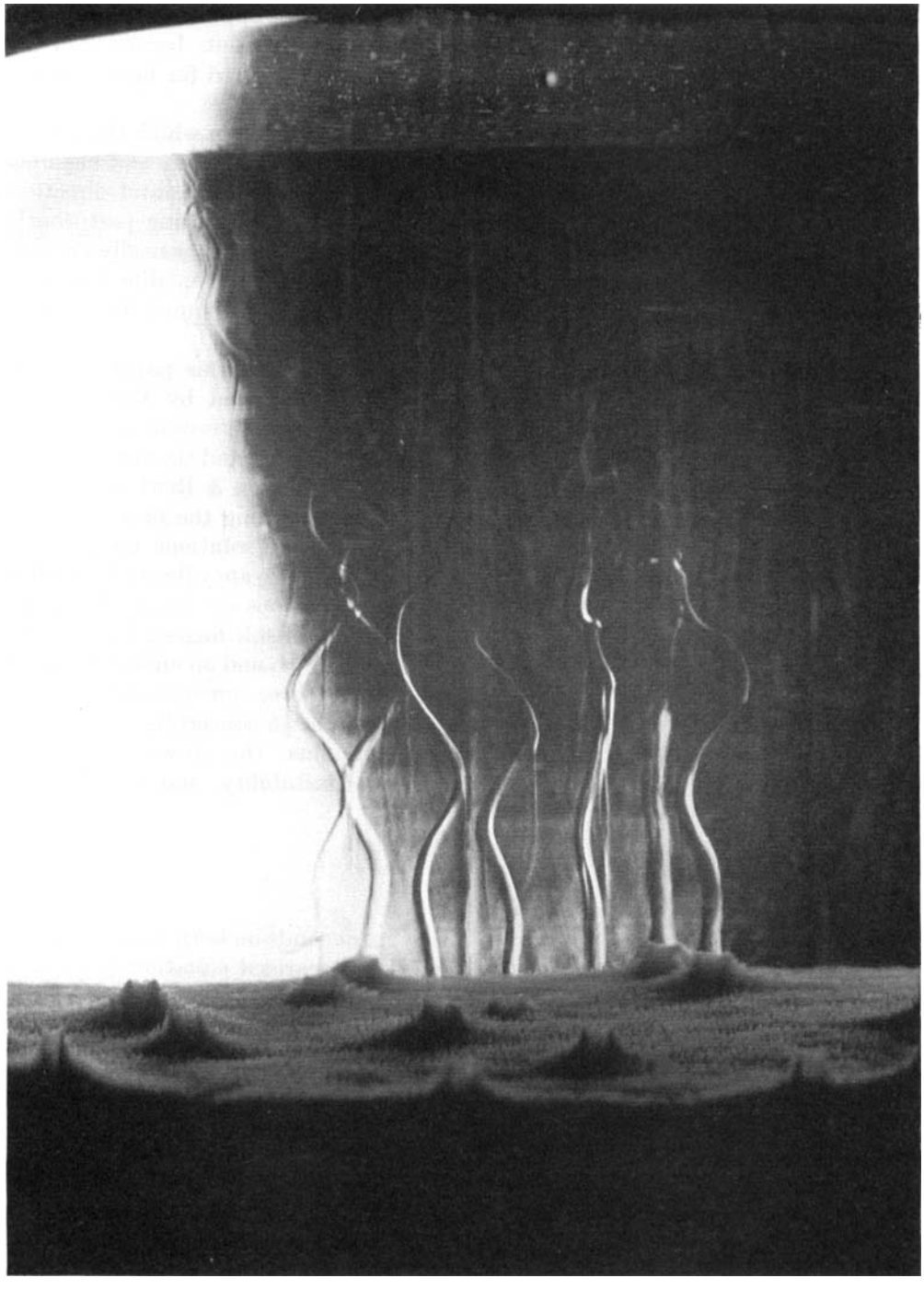

FIGURE 1. Plumes of fresh water emanate from chimneys which form spontaneously within a porous matrix of NH_4Cl crystals when a warm aqueous solution of ammonium chloride and water is cooled from below. The compositionally buoyant plumes exhibit a helical instability.

presence of the vertical temperature gradient rules out the applicability of Squire's theorem for parallel flows, as Gill & Davey (1969) pointed out. Indeed it will be shown below that three-dimensional perturbations are preferred for most values of the Prandtl number.

Holyer (1983) has studied another related stability problem in which the medium is infinite but there is no discontinuity. The basic state is stationary and has linear temperature and salinity gradients in both the vertical and horizontal directions. Viscous, thermal and saline diffusions are all included. The resulting perturbation equations possess constant coefficients. The instability isolated is basically the same as that identified by investigators of the rigid-wall problem but modified by saline diffusion and by the absence of the vertical wall. Holyer also examined the nonlinear development of the instability.

It should be noted that the stability problem studied in this paper has some similarities to the stability of parallel shear flows, modified by the effects of buoyancy. Specifically the present problem may be characterized as a viscous parallel-jet flow with an inflexion point, having compositional and thermal buoyancy forces acting parallel to the undisturbed interface (see Drazin & Reid 1981).

This paper is organized as follows. The equations governing the basic-state flow and the perturbations are developed in §2. The analytic solutions for the three geometries are present in §3, and the heat, material and buoyancy fluxes for each are calculated. These exact solutions of the Boussinesq equations are complementary to those presented by Howard & Veronis (1987) of arrays of salt fingers. The stability of the single plane interface is analysed and discussed in §4, and an energy argument is developed to illustrate some of the physics of the new three-dimensional instability found in this section. Some final comments are made in §5 concerning the counter-intuitive property that plumes have no net mass flux, the growth rate of the instability, the mechanics of the three-dimensional instability, and the neglect of material diffusivity.

2. Formulation

We consider a Boussinesq fluid whose density, ρ, depends on both temperature, T, and concentration, C, of a buoyant material. The linearized equation of state for density is

$$\rho/\rho_0 = 1-\alpha(T-T_0)-\beta(C-C_0), \tag{2.1}$$

where α is the coefficient of thermal expansion, β is the coefficient of compositional expansion and a subscript 0 denotes a constant reference value. The fluid has finite kinematic viscosity, ν, and thermal diffusivity, κ, but the material diffusivity is assumed to be negligibly small. The equations governing the conservation of mass, momentum, energy and buoyant material are

$$\boldsymbol{\nabla}\cdot\boldsymbol{u} = 0, \tag{2.2}$$

$$\rho_0[\partial\boldsymbol{u}/\partial t+(\boldsymbol{u}\cdot\boldsymbol{\nabla})\boldsymbol{u}] = -\boldsymbol{\nabla}p+\rho_0\nu\nabla^2\boldsymbol{u}-\rho g\hat{\boldsymbol{z}}, \tag{2.3}$$

$$\partial T/\partial t+\boldsymbol{u}\cdot\boldsymbol{\nabla}T = \kappa\nabla^2 T, \tag{2.4}$$

$$\partial C/\partial t+\boldsymbol{u}\cdot\boldsymbol{\nabla}C = 0, \tag{2.5}$$

where $\boldsymbol{u}$ is the velocity vector, p is the pressure, g is the local acceleration of gravity and $\hat{\boldsymbol{z}}$ is an upward unit vector.

Localized fluid motions are imposed on a static state characterized by a uniform composition, C_0, and a uniform temperature gradient

$$\gamma = \mathrm{d}T/\mathrm{d}z. \tag{2.6}$$

We shall assume that $\alpha\gamma > 0$ so that the static state is thermally stably stratified. In the discussion we shall implicitly assume $\alpha > 0$ for ease of interpretation, although the analysis is valid for $\alpha < 0$ as well. Fluid motions will be induced by prescribing a difference on concentration of magnitude $\tilde{C}$ to fluid elements initially lying on either side of a vertical interface. A compensatory difference in temperature of magnitude $-\beta\tilde{C}/\alpha$ is simultaneously imposed far from the interface so that no difference in density is imposed.

The conservation equations may be cast in dimensionless form by choosing $(\nu\kappa/\alpha\gamma g)^{\frac{1}{4}}$, $(\kappa/\alpha\gamma\nu g)^{\frac{1}{2}}$, $\tilde{C}$, $\beta\tilde{C}(g\kappa/\alpha\gamma\nu)^{\frac{1}{2}}$, $\beta\tilde{C}/\alpha$ and $\rho_0\beta\tilde{C}(g^3\nu\kappa/\alpha\gamma)^{\frac{1}{4}}$ as measures of length, time, compositional difference, velocity, temperature difference and pressure difference, respectively. This lengthscale is equivalent to that encountered in the salt-finger regime of a double-diffusive system (see equation (8.1.13) of Turner 1973 and equation (4) of Howard & Veronis 1987). The scalings used here for velocity and temperature differ from those of Howard & Veronis (1987) by their factor Q. Using (2.1), the dimensionless forms of (2.2)–(2.5) are

$$\nabla\cdot\boldsymbol{u} = 0, \tag{2.7}$$

$$\partial\boldsymbol{u}/\partial t + R(\boldsymbol{u}\cdot\nabla)\boldsymbol{u} = -\nabla(p + z/\beta\tilde{C}) + \nabla^2\boldsymbol{u} + (C - C_0 + T - T_0)\hat{\boldsymbol{z}}, \tag{2.8}$$

$$\sigma[\partial T/\partial t + R\boldsymbol{u}\cdot\nabla T] = \nabla^2 T, \tag{2.9}$$

$$\partial C/\partial t + R\boldsymbol{u}\cdot\nabla C = 0, \tag{2.10}$$

where the Prandtl number, σ, and the Reynolds number, R, are defined by

$$\sigma = \nu/\kappa, \quad R = \beta\tilde{C}(g\kappa^3/\alpha^3\gamma^3\nu^5)^{\frac{1}{4}}. \tag{2.11}$$

The flow is forced by the compositional jump $\tilde{C}$ or, equivalently, the parameter R. In what follows we seek to identify the instability which occurs for the smallest possible value of R, and shall find a new type of three-dimensional instability which occurs for any non-zero value of R.

In the absence of forcing, (2.7)–(2.10) admit a static solution

$$\boldsymbol{u} = \boldsymbol{0}, \quad C = C_0, \quad T = T_0 + \frac{z - z_0}{\sigma R}, \quad p = p_0 - \frac{z - z_0}{\beta\tilde{C}} + \frac{(z - z_0)^2}{2\sigma R}. \tag{2.12}$$

We wish to study the stability of various simple steady solutions of (2.7)–(2.10) which are driven by prescribed differences in composition. To that end we shall divide the dimensionless variables into a *static state*, given by (2.12), a steady *basic state*, driven by the forcing and denoted by an overbar, and a *perturbation* of infinitesimal amplitude, ϵ, denoted by a dagger:

$$\left.\begin{aligned} &\boldsymbol{u} = \bar{w}\hat{\boldsymbol{z}} + \epsilon\boldsymbol{u}^\dagger, \quad C = C_0 + \bar{C} + \epsilon C^\dagger, \\ &T = T_0 + (z - z_0)/\sigma R + \bar{T} + \epsilon T^\dagger, \\ &p = p_0 - (z - z_0)/\beta\tilde{C} + (z - z_0)^2/2\sigma R + \bar{p} + \epsilon p^\dagger. \end{aligned}\right\} \tag{2.13}$$

In all cases to be considered the basic state has only a vertical velocity and the basic-state variables are independent of height and time.

Substitution of (2.13) into (2.7)–(2.10) and expansion in powers of ϵ yields the basic-state equations to order ϵ^0 and the linearized perturbation equations to order ϵ^1. The basic-state equations are

$$\mathbf{0} = -\nabla\bar{p} + [\nabla_{\mathrm{H}}^2\bar{w} + \bar{C} + \bar{T}]\hat{\boldsymbol{z}}, \tag{2.14}$$

$$\bar{w} = \nabla_{\mathrm{H}}^2\bar{T}, \tag{2.15}$$

where $\nabla_{\mathrm{H}}^2 = \nabla^2 - \partial^2/\partial z^2$. Note that the two mass conservation equations (2.7) and (2.10) are identically satisfied to this order. The perturbation equations are

$$\nabla\cdot\boldsymbol{u}^\dagger = 0, \tag{2.16}$$

$$\partial\boldsymbol{u}^\dagger/\partial t + R[\bar{w}\,\partial\boldsymbol{u}^\dagger/\partial z + (\boldsymbol{u}^\dagger\cdot\nabla\bar{w})\hat{\boldsymbol{z}}] = -\nabla p^\dagger + \nabla^2\boldsymbol{u}^\dagger + (C^\dagger + T^\dagger)\hat{\boldsymbol{z}}, \tag{2.17}$$

$$\sigma\,\partial T^\dagger/\partial t + \sigma R[\bar{w}\,\partial T^\dagger/\partial z + \boldsymbol{u}^\dagger\cdot\nabla\bar{T}] + \boldsymbol{u}^\dagger\cdot\hat{\boldsymbol{z}} = \nabla^2 T^\dagger, \tag{2.18}$$

$$\partial C^\dagger/\partial t + R\bar{w}\,\partial C^\dagger/\partial z = 0. \tag{2.19}$$

Both the barred and daggered variables are subject to the conditions that values and fluxes are continuous and that the variables decay with distance from any localized region of forcing (to be specified).

It is readily seen from (2.14) and $\bar{p}$ must vary linearly with vertical distance z unless

$$\nabla_{\mathrm{H}}^2\bar{w} + \bar{C} + \bar{T} = 0. \tag{2.20}$$

Since the fluid far from the interface has been assumed to be in hydrostatic equilibrium, such a variation of $\bar{p}$ is ruled out and we must assume that (2.20) holds. Now $\bar{p} = 0$ and the basic state is governed by (2.15) and (2.20), which are to be solved for $\bar{w}$ and $\bar{T}$, once $\bar{C}$ is prescribed. These two equations may be compactly combined into a single second-order complex equation:

$$\nabla_{\mathrm{H}}^2 Y - \mathrm{i}Y = \mathrm{i}\bar{C}, \tag{2.21}$$

where

$$Y = \bar{T} - \mathrm{i}\bar{w} \tag{2.22}$$

and $\mathrm{i} = \sqrt{-1}$. Equation (2.21) is equivalent to Howard &Veronis (1987, equation (7)).

3. Some basic-state solutions

In this section we present basic-state solutions driven by prescribed compositional jumps across three vertical interfaces: a single plane interface, two parallel interfaces with equal and opposite jumps (i.e. a Cartesian plume) and a circular cylindrical interface (i.e. a cylindrical plume). The last case is believed to have the greatest potential for physical application, but the planar examples are instructive and will be presented first.

3.1. *Single plane interface*

To maintain symmetry in the solution, let

$$\bar{C} = -\tfrac{1}{2}\mathrm{sgn}\,(x) \tag{3.1}$$

in a Cartesian system of coordinates $Oxyz$ with Oz being vertically upward, Ox horizontal and perpendicular to the interface and Oy horizontal along the undisplaced

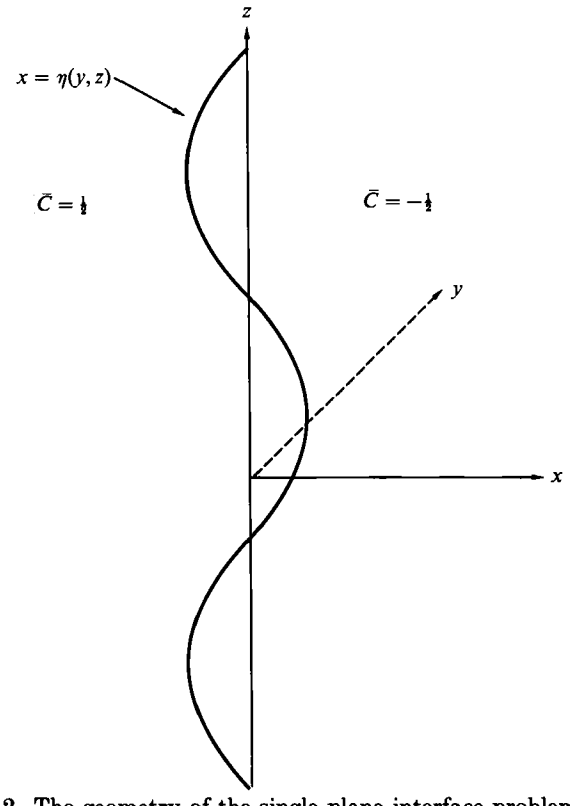

FIGURE 2. The geometry of the single-plane-interface problem.

interface. There is a (dimensional) jump in composition of unit magnitude at $x = 0$ such that the compositionally more buoyant fluid occurs in $x < 0$ and the more dense is in $0 < x$ (see figure 2).

The basic-state variables $\bar{w}$ and $\bar{T}$ depend only on the coordinate x normal to the interface so that $\nabla_{\mathrm{H}}^2 = \mathrm{d}^2/\mathrm{d}x^2$ and (2.21) becomes

$$\frac{\mathrm{d}^2 Y}{\mathrm{d}x^2} - \mathrm{i}Y = -\tfrac{1}{2}\mathrm{i}\,\mathrm{sgn}\,(x). \tag{3.2}$$

The auxiliary conditions are that Y and $\mathrm{d}Y/\mathrm{d}x$ are continuous at $x = 0$ and that Y is finite as $|x| \to \infty$. The solution of (3.2) satisfying these conditions is

$$Y = \tfrac{1}{2}(\mathrm{sgn}\,(x))\,[1 - \exp\,(-k|x|)], \tag{3.3}$$

where

$$k = \frac{1+\mathrm{i}}{\sqrt{2}}. \tag{3.4}$$

Using (2.22) the vertical velocity and temperature are

$$\bar{w} = -\tfrac{1}{2}\exp\left(-\frac{|x|}{\sqrt{2}}\right)\sin\left(\frac{x}{\sqrt{2}}\right), \tag{3.5}$$

$$\bar{T} = \tfrac{1}{2}\left[1 - \exp\left(-\frac{|x|}{\sqrt{2}}\right)\cos\left(\frac{x}{\sqrt{2}}\right)\right]\mathrm{sgn}\,(x). \tag{3.6}$$

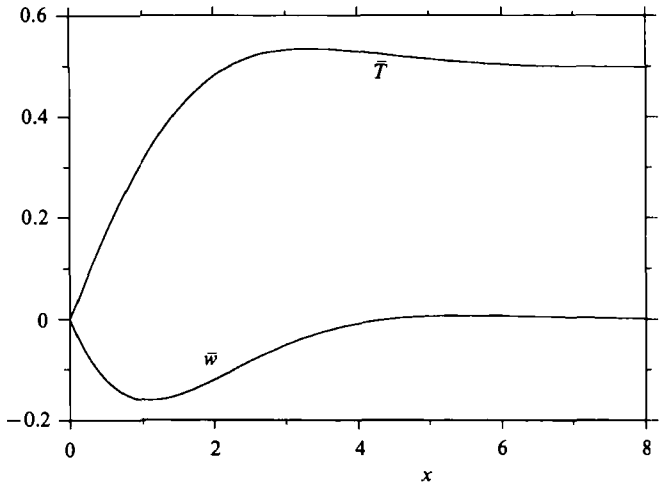

FIGURE 3. The basic-state vertical velocity, $\bar{w}$, and temperature, T, plotted versus distance, x, from the interface from the single plane interface. Both are odd functions of x.

Note that both $\bar{w}$ and $\bar{T}$ are odd functions of x. These are plotted versus x for $0 < x$ in figure 3. Solutions (3.5) and (3.6) are equivalent to (4.9) and (4.10) of Gill (1966), and solutions (8a) and (8b) of Howard & Veronis (1987) reduce to (3.5) and (3.6) in the limit $b \to \infty$.

In this configuration the basic-state temperature approaches a non-zero value of $\frac{1}{2}\mathrm{sgn}(x)$ as $|x| \to \infty$. This is necessary to counterbalance the effect of the prescribed jump in composition (3.1) and produce identical densities as $x \to \pm\infty$. The flow is principally upward for $x < 0$ where the lighter fluid occurs, as one would expect. The dimensional upward mass flux for $x < 0$ is $\nu R/2\sqrt{2}$. There is a downward flux of equal magnitude for $0 < x$; the net vertical mass flux is zero.

An unexpected feature of the flow is its oscillatory character with upward motion of compositionally dense fluid for $(2n-1)\pi < x/\sqrt{2} < 2n\pi$. This feature is common to all basic-state solutions and may be explained as follows. The downward motion of dense fluid in $0 < x/\sqrt{2} < \pi$ advects warmer fluid from above; the static state has (with $\alpha > 0$) warmer fluid lying above colder. This advection is reflected in the large negative gradient $\mathrm{d}\bar{T}/\mathrm{d}x$ in this interval. An antisymmetrical upward flow of cold fluid in $-\pi < x/\sqrt{2} < 0$ maintains the gradient near $x = 0$, but thermal diffusion in the positive-x direction combined with the advection causes the fluid lying in $\pi/2 < x/\sqrt{2} < 3\pi/2$ to be warmer than that at $x = \infty$. This warmer buoyant fluid tends to rise, with upward flow occurring in $\pi < x/\sqrt{2} < 2\pi$. This upward flow advects colder fluid from below and the process repeats with opposite sign and diminished amplitude at larger values of x. This oscillatory character of the flow adjacent to a single interface is closely related to the tendency of 'too-wide' salt fingers to split apart, as discussed by Howard & Veronis (1987).

3.2. *Two parallel interfaces*

Let us now suppose that compositionally buoyant (or dense) material occurs within a vertical planar region of thickness $2x_0$. Taking the same coordinate system as in §3.1, $\bar{C}$ has the top-hat profile

$$\bar{C} = \begin{cases} 1 & \text{for} \quad |x| < x_0 \\ 0 & \text{for} \quad x_0 < |x|. \end{cases} \tag{3.7}$$

Note that a new dimensionless parameter, x_0, has been introduced; it measures the thickness of the plume relative to the salt-finger lengthscale, $(\nu\kappa/\alpha\gamma g)^{\frac{1}{4}}$.

Again assuming $\bar{w}$ and $\bar{T}$ depend only on x, (2.21) becomes

$$\frac{\mathrm{d}^2Y}{\mathrm{d}x^2} - \mathrm{i}Y = \begin{cases} \mathrm{i} & \text{for} \quad |x| < x_0 \\ 0 & \text{for} \quad x_0 < |x|. \end{cases} \tag{3.8}$$

The auxiliary conditions are that Y and $\mathrm{d}Y/\mathrm{d}x$ are continuous at $|x| = x_0$ and that Y is finite as $|x| \to \infty$. The solution of (3.8) satisfying these conditions is:

$$Y = \begin{cases} \exp(-kx_0)\cosh(kx) - 1 & \text{for} \quad |x| < x_0 \\ -\exp(-k|x|)\sinh(kx_0) & \text{for} \quad x_0 < |x|. \end{cases} \tag{3.9}$$

Unified real expressions for $\bar{w}$ and $\bar{T}$ are

$$\bar{w}(x;x_0) = \tfrac{1}{2}[\exp(-X_+)\sin(X_+) - \exp(-|X_-|)\sin(X_-)], \tag{3.10}$$

$$\bar{T}(x;x_0) = \tfrac{1}{2}\{[\exp(-X_+)\cos(X_+) - 1] - [\exp(-|X_-|)\cos(X_-) - 1]\operatorname{sgn}(X_-)\}, \tag{3.11}$$

where

$$X_\pm = (|x| \pm x_0)/\sqrt{2}. \tag{3.12}$$

Note that Y and hence $\bar{w}$ and $\bar{T}$ are even functions of x. $\bar{w}$ and $\bar{T}$ are plotted versus x for $0 < x$ in figure 4 for various values of the plume thickness x_0.

Solutions (3.10) and (3.11) are essentially two solutions of the form (3.5) and (3.6) superposed. In the limit $x_0 \to \infty$, they become two separate solutions. An interesting feature of the flow is that there is no net vertical mass flux in spite of the positive buoyancy perturbation. Upward flow within the plume is balanced by downward flow adjacent to it.

The values of $\bar{w}$ and $\bar{T}$ on the axis of the plume are

$$\bar{w}(0;x_0) = \exp(-x_0/\sqrt{2})\sin(x_0/\sqrt{2}), \tag{3.13}$$

$$\bar{T}(0;x_0) = \exp(-x_0/\sqrt{2})\cos(x_0/\sqrt{2}) - 1. \tag{3.14}$$

These are functionally equivalent to the single-interface solutions (3.5) and (3.6) shown in figure 3, the only difference being a doubling of the amplitude. The values of these variables at the compositional interface, $x = x_0$, are

$$\bar{w}(x_0;x_0) = \tfrac{1}{2}\exp(-\sqrt{2}x_0)\sin(\sqrt{2}x_0), \tag{3.15}$$

$$\bar{T}(x_0;x_0) = \tfrac{1}{2}[\exp(-\sqrt{2}x_0)\cos(\sqrt{2}x_0) - 1]. \tag{3.16}$$

Again, the graphs of these are equivalent to the curves given in figure 3, if the horizontal scale is halved.

3.3. *Cylindrical interface*

Now consider compositionally buoyant material within a circular cylindrical surface of radius s_0:

$$\bar{C} = \begin{cases} 1 & \text{for} \quad 0 < s < s_0 \\ 0 & \text{for} \quad s_0 < s, \end{cases} \tag{3.17}$$

where s is a horizontal radial coordinate.

Assuming $\bar{w}$ and $\bar{T}$ depend only on s, (2.21) becomes

$$\frac{\mathrm{d}^2Y}{\mathrm{d}s^2} + \frac{\mathrm{d}Y}{s\,\mathrm{d}s} - \mathrm{i}Y = \mathrm{i}\bar{C}. \tag{3.18}$$

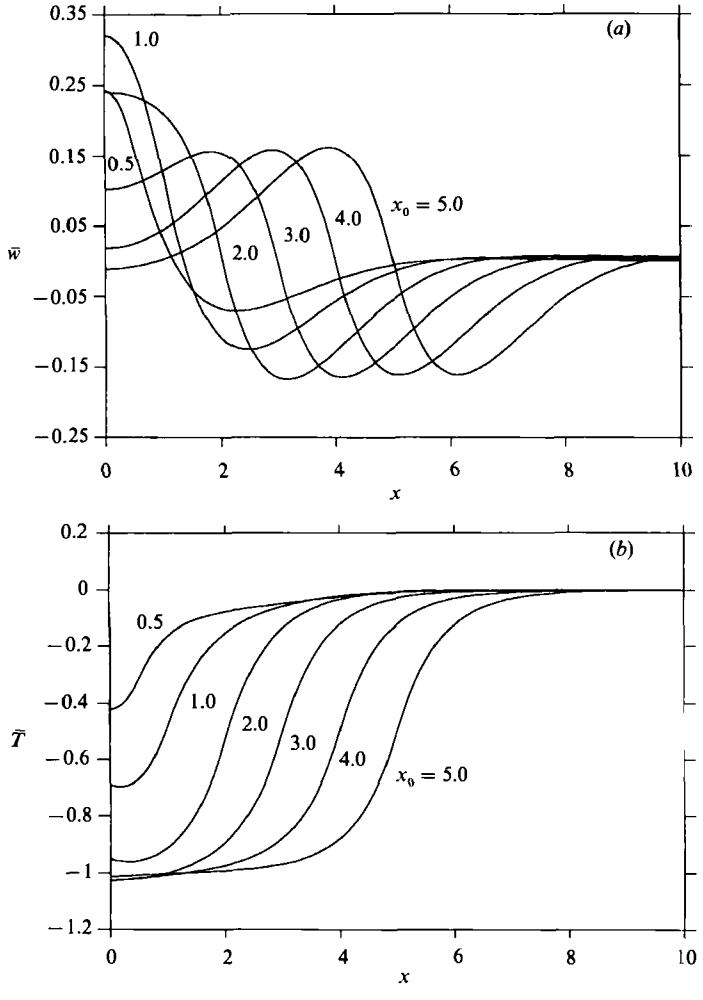

FIGURE 4. (*a*) The basic-state vertical velocity, $\bar{w}$, and (*b*) temperature, $\bar{T}$, plotted versus distance, x, from the axis of symmetry of the top-hat Cartesian plume, for values 0.5, 1.0, 2.0, 3.0, 4.0 and 5.0 of the plume thickness, x_0. Note that the graphs of $\bar{w}(x-x_0)$ and $\bar{T}(x-x_0)+0.5$ approach those of figure 3 as x_0 increases.

The auxiliary conditions are that $\mathrm{d}Y/\mathrm{d}s = 0$ at $s = 0$, Y and $\mathrm{d}Y/\mathrm{d}s$ are continuous at $s = s_0$ and Y is finite as $s \to \infty$. The solution of (3.18) satisfying these conditions is

$$Y = \begin{cases} -s_0[\mathrm{Ker}'(s_0)+\mathrm{i}\,\mathrm{Kei}'(s_0)][\mathrm{Ber}(s)+\mathrm{i}\,\mathrm{Bei}(s)]-1 & \text{for} \quad s < s_0 \\ -s_0[\mathrm{Ber}'(s_0)+\mathrm{i}\,\mathrm{Bei}'(s_0)][\mathrm{Ker}(s)+\mathrm{i}\,\mathrm{Kei}(s)] & \text{for} \quad s_0 < s, \end{cases} \tag{3.19}$$

where Ber, Bei, Ker and Kei are the usual Kelvin functions (see Abramowitz & Stegun 1965, Chapter 9) and a prime denotes differentiation with respect to the argument.

Using the asymptotic properties of the Kelvin functions for large argument,

$$\mathrm{Ber}(z)+\mathrm{i}\,\mathrm{Bei}(z) = I_0(kz) \sim (2\pi kz)^{-\frac{1}{2}}\exp(kz),$$

$$\mathrm{Ker}(z)+\mathrm{i}\,\mathrm{Kei}(z) = K_0(kz) \sim (\pi/2kz)^{\frac{1}{2}}\exp(-kz),$$

it may be verified that (3.19) becomes equivalent to (3.3) in the limit $s_0 \to \infty$; the only difference being the factor $\frac{1}{2}\operatorname{sgn}(s-s_0)$ due to the difference in the zero level between (3.1) and (3.17).

The velocity and temperature for this cylindrical plume may be expressed as

$$\bar{w}(s;s_0) = \begin{cases} A_0 \operatorname{Bei}(s) + B_0 \operatorname{Ber}(s) & \text{for} \quad s < s_0 \\ D_0 \operatorname{Ker}(s) + C_0 \operatorname{Kei}(s) & \text{for} \quad s_0 < s, \end{cases} \tag{3.20}$$

$$\bar{T}(s;s_0) = \begin{cases} -A_0 \operatorname{Ber}(s) + B_0 \operatorname{Bei}(s) - 1 & \text{for} \quad s < s_0, \\ -C_0 \operatorname{Ker}(s) + D_0 \operatorname{Kei}(s) & \text{for} \quad s_0 < s, \end{cases} \tag{3.21}$$

where

$$\left.\begin{aligned} A_0 &= s_0 \operatorname{Ker}'(s_0), \quad B_0 = s_0 \operatorname{Kei}'(s_0), \\ C_0 &= s_0 \operatorname{Ber}'(s_0), \quad D_0 = s_0 \operatorname{Bei}'(s_0). \end{aligned}\right\} \tag{3.22}$$

The graphs of $\bar{w}$ and $\bar{T}$ versus s for several values of s_0 are given in figure 5.

3.4. *Heat, material and buoyancy fluxes*

Following Howard & Veronis (1987; hereinafter referred to as H&V), we may define fluxes of heat, material and buoyancy per unit length of interface:

$$F_{\mathrm{H}} = \frac{1}{L}\int wT \,\mathrm{d}A, \quad F_{\mathrm{m}} = \frac{1}{L}\int wC \,\mathrm{d}A, \quad F_{\mathrm{B}} = \alpha F_{\mathrm{H}} + \beta F_{\mathrm{m}}, \tag{3.23}$$

where the integrals are taken over a specified horizontal area and L is a measure of the horizontal length of the interface. (Since C here is a measure of buoyant material whereas s is a measure of dense material in H&V, there is a sign difference between the definition of the buoyancy flux in (3.23) and that used by H&V. Also the fluxes of these isolated interfaces are normalized by horizontal length of interface rather than area as in H&V.) Non-dimensionalizing these fluxes with $\beta^2\tilde{C}^2(g\kappa^3/\nu\alpha^3\gamma^3)^{\frac{1}{4}}$, $\beta\tilde{C}^2(g\alpha\kappa^3/\nu\gamma^3)^{\frac{1}{4}}$ and $\beta^2\tilde{C}^2(g\alpha\kappa^3/\nu\gamma^3)^{\frac{1}{4}}$, respectively, and noting that by conservation of mass the vertical advection of the static state produces no flux, we may write

$$\tilde{F}_{\mathrm{H}} = \frac{1}{L}\int \bar{w}\bar{T} \,\mathrm{d}A, \quad \tilde{F}_{\mathrm{m}} = \frac{1}{L}\int \bar{w}\bar{C} \,\mathrm{d}A, \quad \tilde{F}_{\mathrm{B}} = \tilde{F}_{\mathrm{H}} + \tilde{F}_{\mathrm{m}}. \tag{3.24}$$

For a single plane interface, we have

$$\tilde{F}_{\mathrm{H}} = \int_{-\infty}^{\infty} \bar{w}\bar{T} \,\mathrm{d}x, \quad \tilde{F}_{\mathrm{m}} = \int_{-\infty}^{\infty} \bar{w}\bar{C} \,\mathrm{d}x, \tag{3.25}$$

with $\bar{C}$, $\bar{w}$ and $\bar{T}$ given by (3.1), (3.5) and (3.6). These integrals yield

$$\tilde{F}_{\mathrm{H}} = -\tfrac{3}{16}\sqrt{2}, \quad \tilde{F}_{\mathrm{m}} = \tfrac{1}{4}\sqrt{2}, \quad \tilde{F}_{\mathrm{B}} = \tfrac{1}{16}\sqrt{2}. \tag{3.26}$$

The flux ratio, F_{r}, for the single interface is

$$F_{\mathrm{r}} = -\tilde{F}_{\mathrm{H}}/\tilde{F}_{\mathrm{m}} = \tfrac{3}{4}. \tag{3.27}$$

For a top-hat Cartesian plume, we must integrate

$$\tilde{F}_{\mathrm{H}} = \frac{1}{2}\int_{-\infty}^{\infty} \bar{w}\bar{T} \,\mathrm{d}x, \quad \tilde{F}_{\mathrm{m}} = \frac{1}{2}\int_{-\infty}^{\infty} \bar{w}\bar{C} \,\mathrm{d}x, \tag{3.28}$$

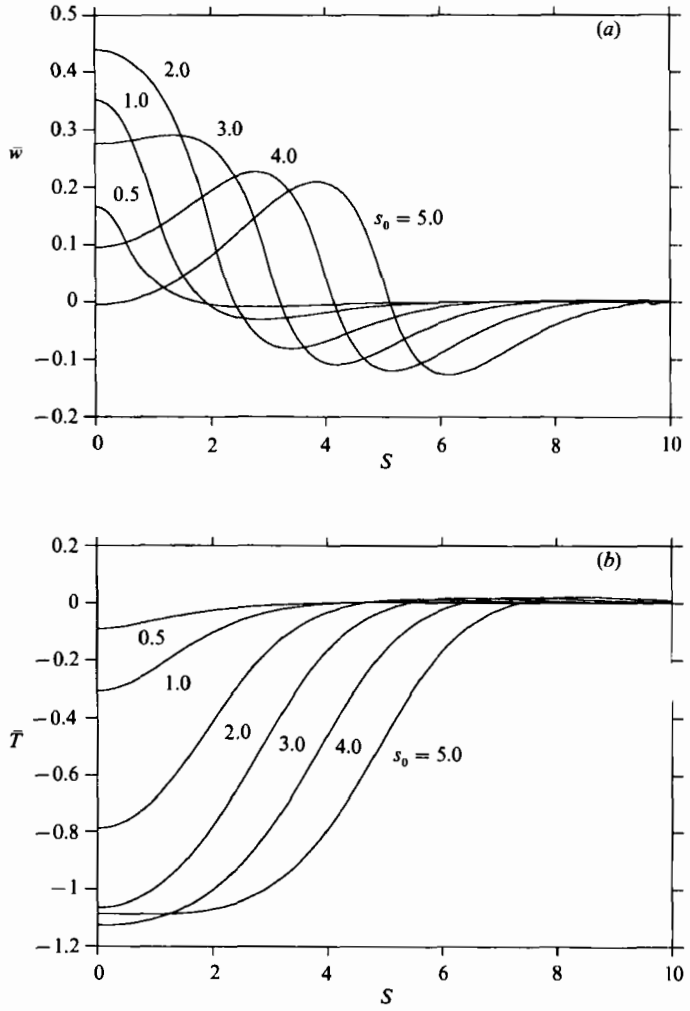

FIGURE 5. (*a*) The basic-state vertical velocity, $\bar{w}$, and (*b*) temperature, $\bar{T}$, plotted versus radius, s, for values 0.5, 1.0, 2.0, 3.0, 4.0 and 5.0 of the radius, s_0, of the cylindrical plume. Note that the graphs of $\bar{w}(s-s_0)$ and $\bar{T}(s-s_0)+0.5$ approach those of figure 3 as s_0 increases.

where the factor of $\frac{1}{2}$ occurs because there are two interfaces per unit length. Integration of (3.28) with $\bar{C}$, $\bar{w}$ and $\bar{T}$ given by (3.7), (3.10) and (3.11) yields

$$\left.\begin{aligned}\tilde{F}_{\mathrm{H}} &= -\tfrac{3}{16}\sqrt{2}+\tfrac{1}{16}\sqrt{2}[3\cos(\sqrt{2x_0})+2\sin(\sqrt{2x_0})]\exp(-\sqrt{2x_0}),\\ \tilde{F}_{\mathrm{m}} &= \tfrac{1}{4}\sqrt{2}-\tfrac{1}{4}\sqrt{2}[\cos(\sqrt{2x_0})+\sin(\sqrt{2x_0})]\exp(-\sqrt{2x_0}),\\ \tilde{F}_{\mathrm{B}} &= \tfrac{1}{16}\sqrt{2}-\tfrac{1}{16}\sqrt{2}[\cos(\sqrt{2x_0})+2\sin(\sqrt{2x_0})]\exp(-\sqrt{2x_0}),\end{aligned}\right\} \tag{3.29}$$

and

$$F_{\mathrm{r}} = \frac{3}{4}+\frac{\sin(\sqrt{2x_0})}{4[\exp(\sqrt{2x_0})-\cos(\sqrt{2x_0})-\sin(\sqrt{2x_0})]}. \tag{3.30}$$

$\tilde{F}_{\mathrm{B}}$ and F_{r} are plotted versus x_0 in figure 6. $\tilde{F}_{\mathrm{B}}$ has local minima at $\sqrt{2x_0} = \arctan\frac{1}{3} + 2n\pi$ and local maxima at $\sqrt{2x_0} = \arctan\frac{1}{3}+(2n+1)\pi$, for $n = 0, 1, 2, \ldots$. The largest of these maxima is that for $n = 0$, giving $x_0 = 2.449$ and $\tilde{F}_{\mathrm{B}} = 0.09277$ and $F_{\mathrm{r}} = 0.7476$. The buoyancy flux per unit area, $\tilde{F}_{\mathrm{B}}/x_0$, is also plotted in figure 6 as a dashed line; this corresponds to the normalization of H&V. This flux has a maximum

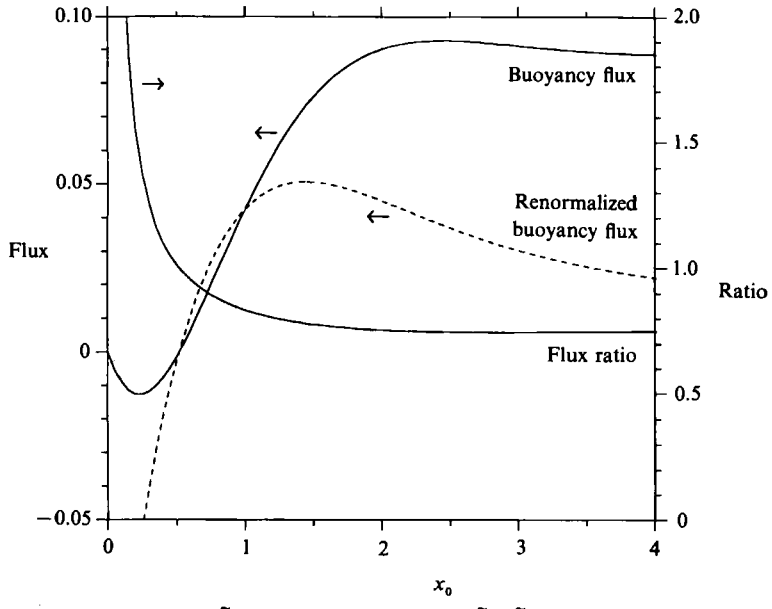

FIGURE 6. The buoyancy flux, $\tilde{F}_B$, and flux ratio $F_r = \tilde{F}_H/\tilde{F}_m$ for the Cartesian plume plotted versus plume thickness, x_0. The area-normalized buoyancy flux, $\tilde{F}_B/x_0$, is plotted as a dashed curve. Note that the buoyancy flux approaches the value of that for the single plane interface (see (3.26)) as x_0 becomes large.

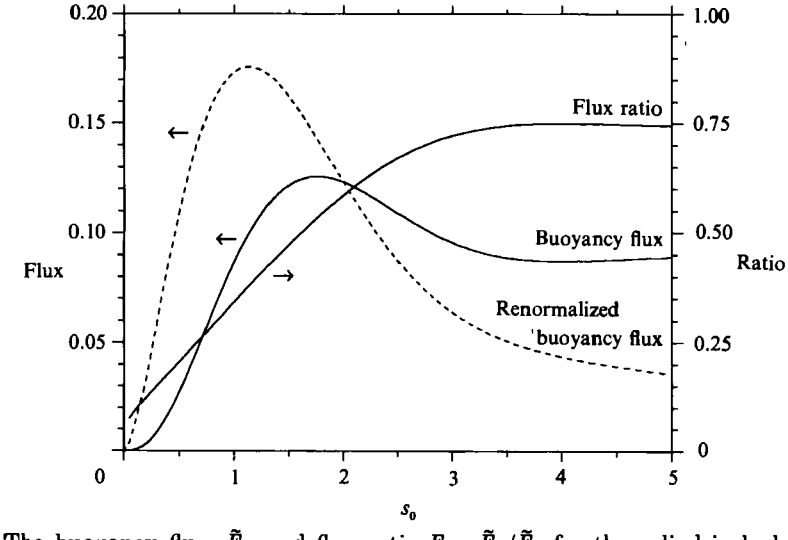

FIGURE 7. The buoyancy flux, $\tilde{F}_B$, and flux ratio $F_r = \tilde{F}_H/\tilde{F}_m$ for the cylindrical plume plotted versus plume radius, s_0. The area-normalized buoyancy flux, $2\tilde{F}_B/s_0$, is plotted as a dashed curve. Note that the buoyancy flux approaches the value of that for the single plane interface (see (3.26)) as s_0 becomes large.

of 0.05066 at $x_0 = 1.445$. The corresponding flux ratio is 0.7806. The area-averaged buoyancy flux is introduced here for comparison with H&V; it is believed that the buoyancy flux $\tilde{F}_B$ is the proper measure of the robustness of the isolated plume. The curves in figure 6 may be compared with those for the planar array in figure 3 of H&V, where $x_0 = \sqrt{2\pi b}$.

Plume type	Thickness†	Buoyancy flux‡	Flux ratio
Single plane	—	0.088388	0.750
Double plane	2.449	0.092766	0.7476
Plane array	2.404	0.135	0.251
Square array	3.479	0.117	0.256
Cylindrical	1.7595	0.1258	0.5349

† In units of $L = (\nu\kappa/g\alpha\gamma)^{\frac{1}{4}}$.
‡ In units of $\beta^2\tilde{C}^2\kappa/\alpha\gamma L^k$ with $k = 1$ for isolated plumes and 2 for arrays.

TABLE 1. Comparison of optimal thickness, which maximizes the buoyancy flux, for several configurations of salt fingers. The flux ratio at optimum is also tabulated.

Note that $\tilde{F}_B$ for the Cartesian plume is negative for $x_0 < 0.5183$. This strongly suggests that such narrow isolated planar plumes cannot exist. This in contrast to the case of a planar array where the buoyancy flux is positive for all values of finger width; see figure 3 of H&V. The negative buoyancy flux results from a quadratic variation of the positive $\tilde{F}_m$ for small x_0, whereas the negative $\tilde{F}_H$ varies linearly. The flux ratio for the Cartesian plume is typically larger than $\frac{3}{4}$ (and larger than 1 for small x_0), in contrast to that of the planar array which is typically less than $\frac{3}{4}$. This indicates that isolated planar plumes are not robust features. This lack of robustness is also indicated by the broad maximum in $\tilde{F}_B$ seen in figure 6, and in the fact that the optimal buoyancy flux for the planar plume is only slightly larger than that for a single plane interface and significantly less than that for a planar array.

To calculate the fluxes for a top-hat cylindrical plume, we must integrate

$$\tilde{F}_H = \frac{1}{s_0}\int_0^\infty \bar{w}\bar{T}s\,\mathrm{d}s, \quad \tilde{F}_m = \frac{1}{s_0}\int_0^{s_0} \bar{w}s\,\mathrm{d}s, \tag{3.31}$$

where $\bar{w}$ and $\bar{T}$ are given by (3.20) and (3.21). Using equations (9.9.21), (9.9.26) and (9.9.27) of Abramowitz & Stegun (1965), these integrals yields

$$\tilde{F}_m = \frac{B_0D_0 - A_0C_0}{s_0}, \tag{3.32}$$

$$\tilde{F}_H = -\tilde{F}_m - \tfrac{1}{2}s_0(A_0^2 - B_0^2)\,\mathrm{Ber}\,(s_0)\,\mathrm{Bei}\,(s_0) - \tfrac{1}{2}s_0A_0B_0(\mathrm{Ber}^2\,(s_0) - \mathrm{Bei}^2\,(s_0)) + \tfrac{1}{2}s_0(C_0^2 - D_0^2)\,\mathrm{Ker}\,(s_0)\,\mathrm{Kei}\,(s_0) + \tfrac{1}{2}s_0C_0D_0(\mathrm{Ker}^2\,(s_0) - \mathrm{Kei}^2\,(s_0)). \tag{3.33}$$

The fluxes $\tilde{F}_B$ and F_r are plotted in figure 7. $\tilde{F}_B$ reaches a maximum of 0.1258 for $s_0 = 1.759$; $F_r = 0.5349$ at that radius. The area-normalized flux $2\tilde{F}_B/s_0$ is plotted in figure 7 as a dashed line. This flux attains a maximum of 0.1760 at $s_0 = 1.134$; $F_r = 0.3782$ at that radius. Comparison of figure 7 with figure 6 shows that the cylindrical plume is much more robust than the Cartesian plume; the flux ratio tends to zero rather than infinity for a small plume and the maximum of buoyancy flux is significantly larger than the asymptotic value.

A comparison of the optimal thicknesses, optimized buoyancy fluxes and flux ratios for a Cartesian plume, a plane array, a square array and a cylindrical plume are presented in table 1; values for the middle two taken from H&V. The values of $\tilde{F}_B$ and F_r for the single interface are included for comparison. The principal difference between these cases is that the isolated interfaces are characterized by relatively large values of the flux ratio whereas the arrays have much smaller optimal values.

A large value of the flux ratio indicates that the negative heat flux is relatively strong and tends to reduce the overall buoyancy flux. Evidently the counterflow in an array acts to severely reduce the heat flux and make the action of an array more efficient than an isolated plume.

4. Stability of the single plane interface

In this section we consider the linear stability of the simplest of the basic-state solutions presented in §3: that for the single plane interface given by (3.5) and (3.6). Specifically we consider the stability of the flow to infinitesimal harmonic perturbations in the position of the interface initially at $x = 0$. Let the deformed interface occur at

$$x = \eta(y, z, t) = \epsilon \exp[\mathrm{i}(my + nz) + \Omega t)] + \text{c.c.}; \tag{4.1}$$

see figure 2. We shall assume that the perturbation velocity, pressure, temperature and composition have the same harmonic variation in y, z, and t; let

$$\{\boldsymbol{u}^\dagger, p^\dagger, T^\dagger, C^\dagger\} = \{\mathrm{i}u, v, w, \mathrm{i}np, T, C\} \exp[\mathrm{i}(my + nz) + \Omega t)] + \text{c.c.} \tag{4.2}$$

In writing (4.2) we have introduced the imaginary unit in the definitions of the pressure and the x-component of velocity in order to simplify the complex character of the variables.

With (4.2), the perturbation equations (2.16)–(2.19) become

$$\mathrm{d}u/\mathrm{d}x + mv + nw = 0, \tag{4.3}$$

$$(\mathrm{d}^2/\mathrm{d}x^2 - a^2 - \bar{\Omega})\, u = n\, \mathrm{d}p/\mathrm{d}x, \tag{4.4}$$

$$(\mathrm{d}^2/\mathrm{d}x^2 - a^2 - \bar{\Omega})\, v = -mnp, \tag{4.5}$$

$$(\mathrm{d}^2/\mathrm{d}x^2 - a^2 - \bar{\Omega})\, w - \mathrm{i}R(\bar{w})' u + C + T = -n^2 p, \tag{4.6}$$

$$(\mathrm{d}^2/\mathrm{d}x^2 - a^2 - \sigma\bar{\Omega})\, T - \mathrm{i}\sigma R(\bar{T})' u - w = 0, \tag{4.7}$$

$$\bar{\Omega} C = 0, \tag{4.8}$$

where

$$\bar{\Omega} = \Omega + \mathrm{i}nR\bar{w}(x) \tag{4.9}$$

is the Doppler-shifted frequency,

$$a^2 = m^2 + n^2 \tag{4.10}$$

is the square of the wavenumber in the (y, z)-plane and a prime indicates differentiation of the basic-state variable with respect to x. Since $\bar{\Omega}$ is a function of x, through its dependence on $\bar{w}$, and does not vanish everywhere, it follows from (4.8) that

$$C = 0. \tag{4.11}$$

Equations (4.3)–(4.7) are to be solved subject to the condition that all perturbation variables decay to zero as $x \to \pm\infty$ (or satisfy the appropriate radiation conditions). Also the variables and their derivatives must satisfy certain compatibility conditions across the interface described by (4.1). These conditions arise from the requirement that the interface be a material surface and that the full variables and the fluxes of momentum and heat be continuous across the interface. Using (4.3) and continuity of velocity, it may be shown that continuity of momentum flux normal to the interface reduces simply to continuity of pressure. Since the basic-state vertical velocity (3.5) has a discontinuous second derivative at $x = 0$, the perturbation vertical velocity must have an offsetting discontinuity in its first derivative. This has

the effect of making the scaled perturbation problem non-homogeneous. The details of the development of this condition are given in Appendix A; the full set of auxiliary conditions is

$$\text{(i)} \qquad u, v, w, p \text{ and } T \text{ decay to zero as } |x| \to \infty, \tag{4.12a}$$

$$\text{(ii)} \qquad u, v, w, p, T, \mathrm{d}v/\mathrm{d}x \text{ and } \mathrm{d}T/\mathrm{d}x \text{ are continuous at } x = 0, \tag{4.12b}$$

$$\text{(iii)} \qquad (\mathrm{d}w/\mathrm{d}x)_{x=0-} = (\mathrm{d}w/\mathrm{d}x)_{x=0+} + 1, \tag{4.12c}$$

$$\text{(iv)} \qquad Ru = -\mathrm{i}\bar{\Omega} \quad \text{at} \quad x = 0. \tag{4.12d}$$

The factor R appears in the fourth condition because the velocity has not been scaled as length divided by time.

The set of equations (4.3)–(4.7) appears to describe four evolution modes since the parameter Ω appears four times. However, it is easily shown that there are in fact only three modes by operating on (4.3) with $(\mathrm{d}^2/\mathrm{d}x^2 - a^2 - \bar{\Omega})$ and making use of (4.4)–(4.6) to obtain

$$(\mathrm{d}^2/\mathrm{d}x^2 - a^2)\, p - T + 2\mathrm{i}R(\bar{w})' u = 0. \tag{4.13}$$

This may be used in place of (4.4). The frequency appears only three times in the set (4.3), (4.5)–(4.7) and (4.13). If we put v and m equal to zero in this set of equations, it reduces to (2.1) and (2.2) of Gill & Davey (1969), but the two sets of equations are subject to differing boundary conditions.

Before proceeding to solve the stability problem, let us examine the stability of the system when the basic compositional jump is absent, i.e. when $\tilde{C} = 0$. In this case there is no distinction between the fluid on either side of the plane $x = 0$. The fluid has a bottom-heavy density profile due to the static-state ($\bar{w} = 0$) temperature gradient. Since $\tilde{C}$ has been used in the non-dimensionalization of the perturbation equations (2.7)–(2.10), we will revert to dimensional quantities here and assume that the x-dependence is $\exp(\mathrm{i}rx)$ since the perturbation equations have constant coefficients in this limit. The dispersion relation then is

$$(\nu h^2 + \Omega)\,[(\nu h^2 + \Omega)(\kappa h^2 + \Omega) h^2 + \alpha\gamma g(r^2 + m^2)] = 0, \tag{4.14}$$

in which $h^2 = a^2 + r^2$. The solutions are

$$\Omega = -\nu h^2, \quad -\tfrac{1}{2}h^2(\nu + \kappa) \pm \frac{1}{2}\left[h^4(\nu - \kappa)^2 - 4\kappa\alpha\gamma g \frac{(r^2 + m^2)}{h^2}\right]^{\frac{1}{2}}. \tag{4.15}$$

It is readily seen that the real part of Ω is negative for all three modes, indicating stability.

This conclusion rests on the presumption that r^2 is positive; that is, the system is stable to body waves. However, in what follows we are interested in edge waves which decay with distance from the interface at $x = 0$. These waves are characterized by negative values of r^2. Of particular interest is the case in which both R and Ω are small and the edge waves satisfy $a^2 = \lambda^2$ or

$$(\lambda^2 - a^2)^3 + \lambda^2 - m^2 = 0, \tag{4.16}$$

to dominant order, where we have replaced r^2 by $-\lambda^2$.

It follows from the fourth of conditions (4.12) that Ω is no larger than $O(R)$ when $R \ll 1$. The expansion in ascending powers of R has the form

$$\{u, v, w, p, T\} = \sum_{\alpha=0}^{\infty} \{u_\alpha, v_\alpha, w_\alpha, p_\alpha, T_\alpha\} R^\alpha, \quad \Omega = \sum_{\alpha=1}^{\infty} \Omega_\alpha R^\alpha. \tag{4.17}$$

In what follows we shall consider a sequence of problems in ascending powers of R in an effort to determine the conditions under which the single plane interface is unstable.

4.1. *The zeroth-order problem*

The zeroth-order problem consists of (4.3), (4.5)–(4.7) and (4.13), with $\bar{\Omega}$ and the terms containing R and C omitted, subject to conditions (4.12). As explained in Appendix B, the solution may be expressed as

$$\{u_0, v_0, w_0, p_0, T_0\} = \sum_{j=1}^{3} \{-n\lambda_j \operatorname{sgn}(x), -mn, \mu_j^3, \mu_j, \mu_j^2\} A_j \exp(-\lambda_j |x|), \tag{4.18}$$

where

$$A_j = \frac{\mu_j^2}{2\lambda_j(3n^2+2\mu_j)}, \tag{4.19}$$

$$\mu_j = \lambda_j^2 - a^2, \tag{4.20}$$

and

$$\mu_j^3 + \mu_j + n^2 = 0. \tag{4.21}$$

Note that (4.21) is equivalent to (4.16). Also

$$\sum_{j=1}^{3} \lambda_j A_j = 0, \quad \sum_{j=1}^{3} \mu_j^3 \lambda_j A_j = \tfrac{1}{2}, \quad \sum_{j=1}^{3} \mu_j^2 \lambda_j A_j = 0,$$

so that u, $\mathrm{d}v/\mathrm{d}x$ and $\mathrm{d}T/\mathrm{d}x$ are continuous at $x = 0$ and the jump in $\mathrm{d}w/\mathrm{d}x$ is unity as required by (4.12). Also note that

$$\Omega_1 = 0. \tag{4.22}$$

To this order the perturbation is neutrally stable, and in fact stationary, for all values of m, n and σ. These zeroth-order modes are the neutral distortion of the basic-state flow which necessarily accompanies the displacement of the interface.

This neutral stability to first order is reminiscent of that for $\sigma = \infty$ found by Gill & Davey (1969), although there is an important difference. Here the neutral first-order mode is stationary whereas that of Gill & Davey (1969) moves with a phase speed greater than the maximum fluid speed.

It is easy to verify that each of the zeroth-order variables given by (4.18) is real, since one of the three modes, μ, is real while the other two are complex conjugates. Also note that u_0 is an odd function of x, while the other four variables are even in x.

The stability of the single plane interface is determined by investigating the first-order perturbations of this neutral distortion.

4.2. *The first-order problem*

To first order in powers of R, (4.3), (4.5)–(4.7) and (4.13) become

$$(\mathrm{d}^2/\mathrm{d}x^2 - a^2) p_1 - T_1 = -2\mathrm{i}(\bar{w})' u_0, \tag{4.23}$$

$$(\mathrm{d}^2/\mathrm{d}x^2 - a^2) w_1 + T_1 + n^2 p_1 = \mathrm{i}n\bar{w} w_0 + \mathrm{i}(\bar{w})' u_0, \tag{4.24}$$

$$(\mathrm{d}^2/\mathrm{d}x^2 - a^2) T_1 - w_1 = \mathrm{i}n\sigma\bar{w} T_0 + \mathrm{i}\sigma(\bar{T})' u_0, \tag{4.25}$$

$$(\mathrm{d}^2/\mathrm{d}x^2 - a^2) v_1 = -mnp_1 + \mathrm{i}n\bar{w} v_0, \tag{4.26}$$

$$\mathrm{d}u_1/\mathrm{d}x = -mv_1 - nw_1. \tag{4.27}$$

The solutions of these equations are subject to the continuity conditions

$$\left.\begin{aligned} w_1(0-) = w_1(0+), \quad p_1(0-) = p_1(0+), \quad T_1(0-) = T_1(0+), \\ \frac{\mathrm{d}w_1}{\mathrm{d}x}(0-) = \frac{\mathrm{d}w_1}{\mathrm{d}x}(0+), \quad \frac{\mathrm{d}T_1}{\mathrm{d}x}(0-) = \frac{\mathrm{d}T_1}{\mathrm{d}x}(0+), \end{aligned}\right\} \tag{4.28}$$

$$v_1(0-) = v_1(0+), \quad \frac{\mathrm{d}v_1}{\mathrm{d}x}(0-) = \frac{\mathrm{d}v_1}{\mathrm{d}x}(0+), \quad u_1(0-) = u_1(0+) = -\mathrm{i}\Omega_2. \tag{4.29}$$

The last of these serves as the dispersion relation for Ω_2, once the other conditions are satisfied.

The solution of this problem, given in Appendix B, results in a dispersion relation which is linear in the Prandtl number σ:

$$\Omega_2 = c_0 + \sigma c_1, \tag{4.30}$$

where
$$c_r = \hat{u}_r - \frac{m}{a}\hat{v}_r + \left[\frac{m^2}{an} - nM_1\right]\hat{w}_r + \left[\frac{m^2}{an} + n^3 M_0\right]\hat{p}_r - nM_2\hat{T}_r, \tag{4.31}$$

for $r = 0, 1$, where
$$M_k = \sum_{j=1}^{3} \frac{\lambda_j \mu_j^{k-1}}{(3n^2 + 2\mu_j)} \tag{4.32}$$

and
$$\hat{y}_r = -\tfrac{1}{2}n \operatorname{Im}\left[\sum_{j=1}^{3} A_j y_{rj}\right], \tag{4.33}$$

for $y = u, v, w, p, T$, and $r = 0, 1$, with

$$\{w_{0j}, p_{0j}, T_{0j}\} = \frac{1}{D_j}[(\mu_j^3 + k\lambda_j)\{\gamma_j^2, 1, \gamma_j\} + 2k\lambda_j\{n^2\gamma_j, -1-\gamma_j^2, n^2\}], \tag{4.34}$$

$$\{w_{1j}, p_{1j}, T_{1j}\} = \frac{[\mu_j^2 - ik\lambda_j]}{D_j}\{-\gamma_j - n^2, \gamma_j, \gamma_j^2\} \tag{4.35}$$

and
$$u_{rj} = \frac{[mv_{rj} + nw_{rj}]}{\lambda_j + k}, \quad v_{0j} = -\frac{mn[1 + p_{0j}]}{\gamma_j}, \quad v_{1j} = -\frac{mnp_{1j}}{\gamma_j}, \tag{4.36}$$

where
$$D_j = \gamma_j^3 + \gamma_j + n^2, \quad \gamma_j = (\lambda_j + k)^2 - a^2. \tag{4.37}$$

4.3. *Stability results and discussion*

The expression (4.30) for Ω_2 has been evaluated numerically as a function of the wavenumber components m and n for positive values of the Prandtl number, σ. The computations show that the single plane interface is unstable for all values of the Prandtl number in the sense that for every value of σ there exists a pair of values (m, n) for which Ω_2 is positive. Naturally some disturbances are damped. In particular when n is large, and the wavelength in the vertical direction $(= 2\pi/n)$ is short, the disturbance is heavily damped by viscous dissipation. Indeed (4.30) yields

$$\Omega_2 \approx -\frac{n^2 m^2}{16a^4} + \frac{13}{64\sqrt{2}a} \quad \text{as} \quad n \to \infty.$$

We see from this that short wavelength two-dimensional motions (in vertical planes normal to the plane of discontinuity, having $m = 0$) are unstable, while three-dimensional motions with similar short vertical wavelength are stable.

For $m, n \leqslant O(1)$, however, Ω_2 is positive for all m and $n\,(\neq 0)$, provided σ does not exceed a certain value $\sigma_c\,(\approx 1.472)$. For $\sigma > \sigma_c$, a region of stability develops in the

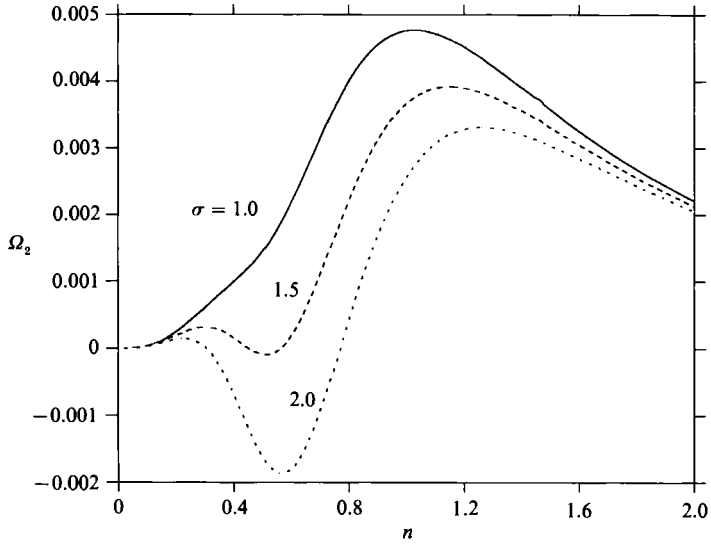

FIGURE 8. The profile of the growth rate Ω_2 of the single plane interface when the horizontal wavenumber $m = 0$ for three different values of the Prandtl number σ near $\sigma = \sigma_c \approx 1.472$, to illustrate the manner in which the region of instability develops with increasing σ for moderate values of the vertical wavenumber n.

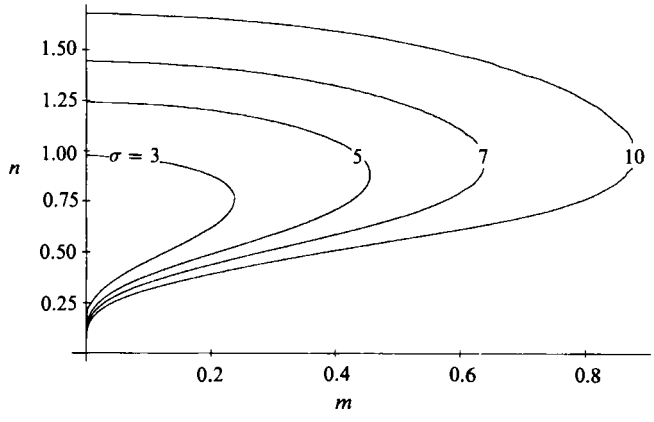

FIGURE 9. The regions of stability for the single plane interface in the (m, n) wavenumber plane for various values of the Prandtl number σ, as labelled. The region of stability lies within the respective curve and instability prevails outside. No stability is possible if $\sigma < 1.472$.

(m, n)-plane for small values of m and moderate values of n. The development of this region of stability is illustrated in figure 8 which shows the profile of the growth rate Ω_2 as a function of n for $m = 0$ and values of σ near the 'critical' value σ_c. For fixed m and $\sigma = 0, \Omega_2(n)$ is positive and has a single maximum at moderate values of n. As σ is increased from zero, a second maximum develops at a smaller value of n. The intervening minimum value of Ω_2 decreases with increasing σ but remains positive provided $\sigma < \sigma_c$. When σ exceeds σ_c, the minimum value of Ω_2 is negative, giving a region of stability for some values of m and n. Further increase in the value of σ results in an enlargement of the stable region, as illustrated in figure 9. The presence of the stable region for moderate values of m and n complicates the isolines of Ω_2 as depicted in figure 10.

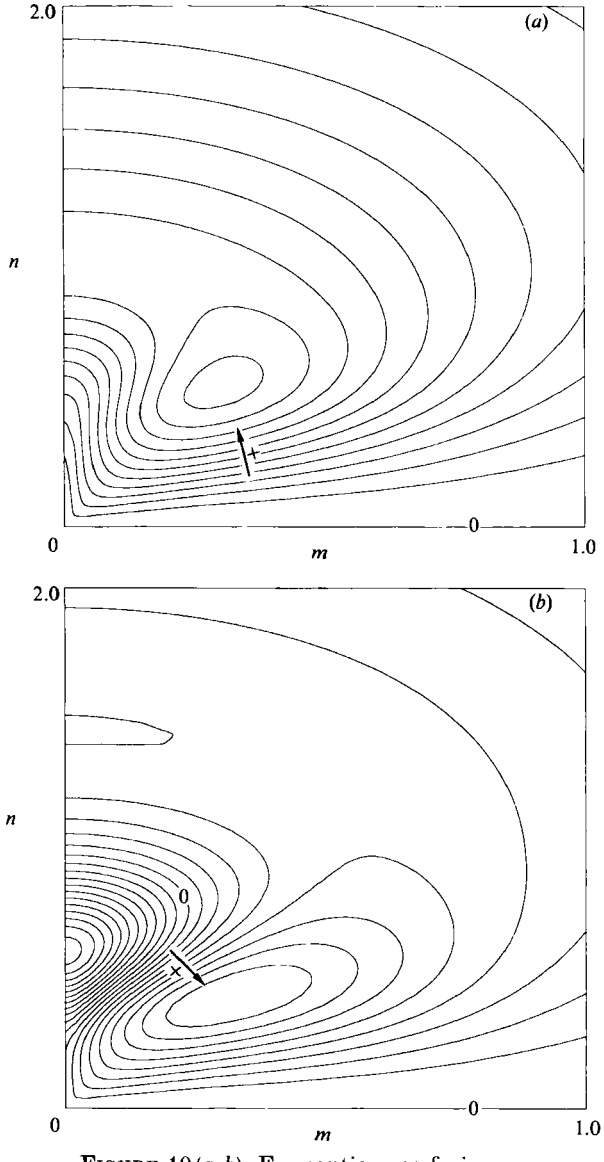

FIGURE 10 (a, b). For caption see facing page.

The increase in the region of stability with increasing σ is due to the stabilizing influence of viscosity, which can be investigated by studying the behaviour of the growth factors c_0 and c_1 in the (m, n)-plane. Noting that $\sigma = \nu/\kappa$, we may interpret c_0 as representing the effect of thermal diffusivity while c_1 represents viscosity. Numerical evaluation of the expression (4.31) for $r = 0$, 1 leads to the isoline plots shown in figure 11 (a, b). It may be seen from this figure that thermal diffusivity promotes instability for all wavenumbers while viscosity is nearly always stabilizing; c_0 is positive for all values of m and n, while c_1 is negative except for n small and m between 0 and 1. c_1 has a maximum of $0.304\,901 \times 10^{-4}$ at $m \approx 0.4971$ and $n \approx 0.2307$.

The mode of primary concern in stability theory is that for which the growth rate Ω_2 is a maximum. This mode, called the *preferred* mode of instability, is identified as

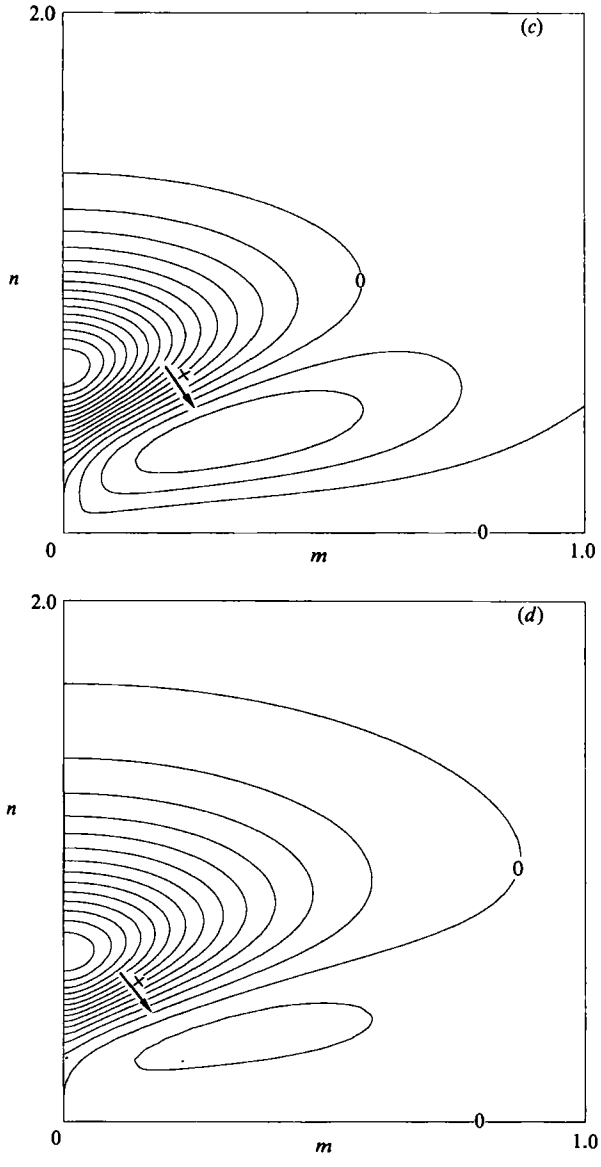

FIGURE 10. Isolines of the growth rate, Ω_2, for the single plane interface for four representative values of the Prandtl number σ: (*a*) $\sigma = 1.0$ (minimum value 0, maximum value 0.00570, contour interval 0.0005); (*b*) $\sigma = 3.0$ (minimum value -0.00580, maximum value 0.00448, contour interval 0.0005); (*c*) $\sigma = 5.0$ (minimum value -0.0139, maximum value 0.00394, contour interval 0.001); (*d*) $\sigma = 10.0$ (minimum value -0.0345, maximum value 0.00336, contour interval 0.0025).

follows. The stationary values of Ω_2 as a function of m and n are determined by solving the equations

$$\partial\Omega_2/\partial m = \partial\Omega_2/\partial n = 0,$$

and (4.31) simultaneously for fixed σ. The preferred mode has the largest stationary value, $\Omega_{2\max}$, of Ω_2. $\Omega_{2\max}$ and the associated values, $m_{\max}$ and $n_{\max}$, of m and n define the preferred mode of instability for that given value of σ. The variation of the preferred mode as a function of σ is illustrated in figure 12. We see that two-

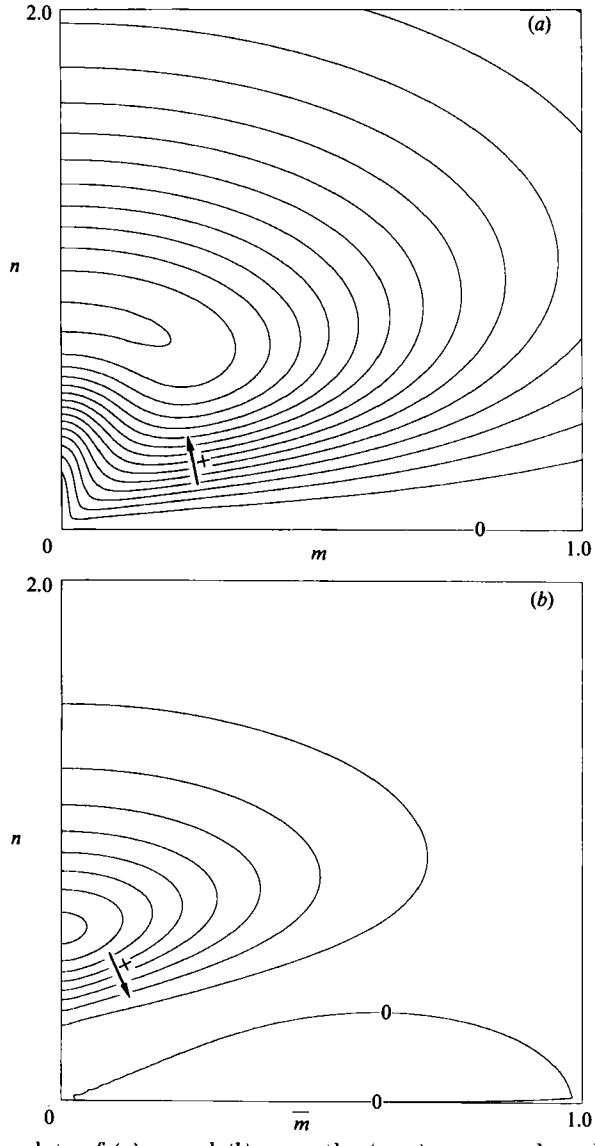

FIGURE 11. Isoline plots of (a) c_0 and (b) c_1 on the (m, n) wavenumber plane for the single line interface. Contour intervals are 0.0005. Minimum value of c_0 is 0, maximum value is 0.00758; minimum value of c_1 is -0.00414, maximum value is 0.0000305.

dimensional motions (i.e. those for which $m = 0$) are preferred only for very small values of the Prandtl number, i.e. for $\sigma \leqslant 0.065$. As σ increases beyond 0.065, $m_{\max}(\sigma)$ increases rapidly with σ until σ reaches about 0.5 and thereafter increases very slowly with σ. On the other hand, $n_{\max}$ increases with σ for two-dimensional motions but decreases with σ for three-dimensional motions. In cases where more than one maximum of Ω_2 occurs, that with the smallest value of $n_{\max}$ is always the largest, reflecting the dissipative role of viscosity. The maximum growth rate, $\Omega_{2\max}$, decreases with σ for values of $\sigma < \sigma_0 (\approx 21.93)$, while for $\sigma > \sigma_0$, $\Omega_{2\max}$ increases slowly with σ. (Similar behaviour was encountered by Gill & Davey (1969) who found that the critical Reynolds number decreases with increasing Prandtl number.) This decrease is due to the increasing influence of the basic-state horizontal gradients of

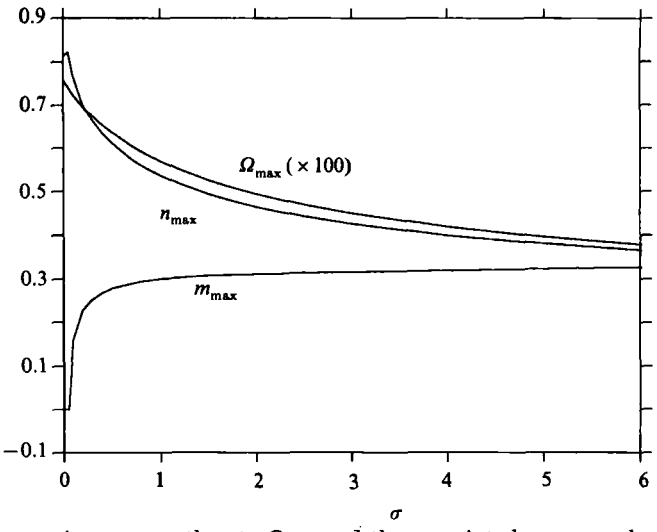

FIGURE 12. The maximum growth rate Ω_{max} and the associated wavenumbers m_{max} and n_{max} for the single plane interface as a function of the Prandtl number σ. Note that $m_{max} = 0$ for $\sigma \leqslant 0.065$.

temperature and velocity. As σ increases, the vertical wavenumber n_{max} decreases (i.e. the vertical wavelength increases) in order to minimize the influence of viscous dissipation, thereby allowing the transfer of energy by the basic-state gradients to offset it and in turn enhance instability.

The present result that three-dimensional motions (i.e. $m \neq 0$) are preferred for almost all values of the Prandtl number, σ, presents a divergence from the results of Holyer (1983). However, the problem studied by Holyer differs from the present problem in two important respects. First, the absence in her problem of a horizontal gradient of vertical velocity rules out any influence of velocity shear. Second, the inclusion of material diffusivity in her problem has the effect of increasing dissipative processes.

4.4. *Energetics of the instability*

In order to identify the driving mechanism for the present instability and clarify the differences with the results of the studies by Gill & Davey (1969), Dudis & Davis (1971) and Holyer (1983), we examine the energetics of the present problem.

The kinetic energy balance is obtained by multiplying (4.4) by u^* (here an asterisk denotes a complex conjugate), (4.5) by v^*, (4.6) by w^* and the conjugate of (4.3) by $-np$, adding the results and integrating over the range of x (and noting that $C = 0$). Separating the result into real and imaginary parts yields

$$\mathrm{Re}\,(\Omega)\,E_M = -D_M + R\,\mathrm{Re}\,(M) + \mathrm{Re}\,(B+J), \tag{4.38a}$$

$$\mathrm{Im}\,(\Omega)\,E_M = -nRE_{WU} + R\,\mathrm{Im}\,(M) + \mathrm{Im}\,(B+J), \tag{4.38b}$$

where

$$\left.\begin{aligned} E_M &= \int_{-\infty}^{\infty} |\boldsymbol{u}|^2\,\mathrm{d}x, \quad D_M = \int_{-\infty}^{\infty}\left[\left|\frac{\mathrm{d}\boldsymbol{u}}{\mathrm{d}x}\right|^2 + a^2|\boldsymbol{u}|^2\right]\mathrm{d}x, \\ M &= -\mathrm{i}\int_{-\infty}^{\infty}\frac{\mathrm{d}\bar{w}}{\mathrm{d}x}uw^*\,\mathrm{d}x, \quad E_{WU} = \int_{-\infty}^{\infty}\bar{w}|\boldsymbol{u}|^2\,\mathrm{d}x, \\ J &= w^*(0)\left[\frac{\mathrm{d}w}{\mathrm{d}x}(0-) - \frac{\mathrm{d}w}{\mathrm{d}x}(0+)\right], \quad B = \int_{-\infty}^{\infty} w^*T\,\mathrm{d}x. \end{aligned}\right\} \tag{4.39}$$

The first term in (4.38) represents the rate of change of wave kinetic energy, D_M represents the rate of viscous dissipation, M the rate of transfer of kinetic energy from the mean flow through the velocity shear, and B and J the rates of gain of wave energy by the actions of buoyancy. B represents the action of thermal buoyancy while J represents the action of compositional buoyancy resulting from the deformation of the interface. Note that $\mathrm{Re}\,(\Omega)\,E_M$, D_M, $R\,\mathrm{Re}\,(M)$ and B in (4.38a) are equivalent to $\alpha Rc_1 E_M$, D_M, RM and B of equation (2.6) of Gill & Davey (1969), but there is no counterpart to J in their problem. Note that for the scaling adopted in this paper, the jump in $\mathrm{d}w/\mathrm{d}x$ is unity so that $J = w^*(0)$.

The thermal energy balance is obtained by multiplying the conjugate of (4.7) by T. The real and imaginary parts are

$$\sigma\,\mathrm{Re}\,(\Omega)\,E_T = -D_T + \sigma R\,\mathrm{Re}\,(H) - \mathrm{Re}\,(B), \tag{4.40a}$$

$$-\sigma\,\mathrm{Im}\,(\Omega)\,E_T = n\sigma R E_{WT} + \sigma R\,\mathrm{Im}\,(H) - \mathrm{Im}\,(B), \tag{4.40b}$$

where

$$\left.\begin{aligned} E_T &= \int_{-\infty}^{\infty} |T|^2\,\mathrm{d}x, \quad D_T = \int_{-\infty}^{\infty} \left[\left|\frac{\mathrm{d}T}{\mathrm{d}x}\right|^2 + a^2|T|^2\right]\mathrm{d}x, \\ H &= \mathrm{i}\int_{-\infty}^{\infty} \frac{\mathrm{d}\bar{T}}{\mathrm{d}x} u^* T\,\mathrm{d}x, \quad E_{WT} = \int_{-\infty}^{\infty} \bar{w}|T|^2\,\mathrm{d}x. \end{aligned}\right\} \tag{4.41}$$

Here E_T represents the gain of wave potential energy, D_T the rate of thermal dissipation and H the rate of transfer of energy from the basic-state thermal profile to the perturbations. The terms of (4.40a) exactly correspond to those of (2.8) of Gill & Davey (1969).

The addition of (4.40a) to (4.38a) and (4.40b) to (4.34b) leads to

$$\mathrm{Re}\,(\Omega)\,[E_M + \sigma E_T] = -(D_M + D_T) + R\,\mathrm{Re}\,(\mathrm{M} + \sigma H) + \mathrm{Re}\,(J), \tag{4.42a}$$

$$\mathrm{Im}\,(\Omega)\,[E_M - \sigma E_T] = nR(E_{WT} - E_{WU}) + R\,\mathrm{Im}\,(M + \sigma H) + \mathrm{Im}\,(J). \tag{4.42b}$$

Equations (4.42a) and (4.42b) show clearly the influence of the discontinuity in the basic compositional concentration, as represented by J, on the growth rate $\mathrm{Re}\,(\Omega)$ and on the frequency $\mathrm{Im}\,(\Omega)$. If $J = 0$ (and the basic compositional concentration is continuous everywhere), then by (4.42a), $\mathrm{Re}\,(\Omega)$ is negative unless $\mathrm{Re}\,(M + \sigma H) > 0$ and R is sufficiently large to overcome the effects of dissipation. In this case, instability is similar to that of the heated-wall problem cited previously. Of course, the values of R giving instability will not be identical with those of the heated-wall problem because the boundary conditions are different; studies of the stability of double-diffusive systems indicate that changes in boundary conditions are, in general, accompanied by only quantitative changes in the stability properties (see, for example, Eltayeb 1972).

If $J \neq 0$, then (4.42a) shows that this new term has the capability of balancing the effects of diffusion even as $R \to 0$. The analysis presented in this paper shows that to order R^0 (for small R) the energy released by deformation of the interface exactly compensates the effects of dissipation:

$$0 = -(D_{M0} + D_{T0}) + w_0^*(0). \tag{4.43}$$

Although the variables do not possess general symmetries with respect to x, since Ω is zero to order R^0 and R^1, the zeroth- and first-order velocities do have symmetries about $x = 0$. In particular, $\boldsymbol{u}_0$ and $\boldsymbol{u}_1$ have opposite symmetries so that the dissipative

terms D_M and D_T are zero to order R. Also with $\bar{w}$, $\bar{T}$ and u_0 odd and v_0, w_0 and T_0 even about $x = 0$, M and H are zero to order R^0. Consequently, (4.42*a*) is to order R, simply

$$0 = w_1^*(0), \tag{4.44}$$

which is consistent with w_1 being an odd function of x. To order R^2, (4.42*a*) yields

$$\mathrm{Re}\,(\Omega_2)\,[E_{M0}+\sigma E_{T0}] = -(D_{M2}+D_{T2}) + \mathrm{Re}\,(M_1+\sigma H_1+w_2^*(0)). \tag{4.45}$$

This shows that the effects of thermal and viscous dissipation may be overcome by a combination of kinetic energy transfer, via M_1, thermal energy transfer, via H_1, and compositional energy transfer, via w_2^*.

5. Final comments

The flow problem studied in the preceding sections has a number of unexpected features which deserve further comment and clarification.

5.1. *Vertical mass flux*

One counter-intuitive property of the three basic-state plume solutions found in §3 is that they each have no net vertical mass flux. Intuitively one would expect a buoyant plume to have a positive vertical mass flux with the return flow at some distance from the plume. That is not the case with the compositionally buoyant plumes studied here. This fact may be verified by integration of (2.15) over the horizontal area of the plume. The single-line interface has no net vertical mass flux by symmetry. The mass fluxes of the top-hat Cartesian and cylindrical plumes may be expressed as

$$\dot{M}_k = \int_0^r r^k \bar{w}\,\mathrm{d}r = \int_0^r (r^k \bar{T}_r)_r\,\mathrm{d}r = r^k \bar{T}_r,$$

where $k = 0$ for the Cartesian plume and 1 for the cylindrical plume. In either case, the vertical mass flux, at an arbitrary distance from the symmetry axis, is directly proportional to the local radial gradient of the basic temperature profile. This gradient must tend to zero as the distance from the plume axis becomes large. Consequently the net vertical mass flux must be zero.

There is no denying that near the axis of the plume a concentrated upward flow of compositionally buoyant fluid occurs. However, the downward return flow does not occur at very large distances, but instead occurs close to the plume. In fact, this return flow is an integral part of the dynamics of the plume. The upward flow near the centre of the plume advects cold fluid from below since the static state is thermally stably stratified. Horizontal diffusion of heat allows this central column of cold buoyant fluid to cool the surrounding fluid which is not compositionally buoyant. This cool dense fluid sinks, contributing substantially to the downward mass flux. This sinking collar of cool fluid drags with it some warmer fluid farther from the plume. This warmer fluid warms the fluid still further from the plume, creating a second weaker updraft, and so on, as described at the end of §3.1.

5.2. *Growth rate of instability*

The flow which has been studied in the preceding sections is forced by the imposed compositional difference, quantified by the dimensionless parameter R. In keeping with the tradition of stability analyses, attention has been focused on the instability

that occurs for the smallest possible value of the forcing R. It was found that, in contrast to the heated-wall problem where instability is possible only if R exceeds some finite critical value R_c, in the present problem instability of the single plane interface is possible for any non-zero value of the forcing. Although the flow is unstable even as $R \to 0$, the timescale for growth of the instability tends to infinity in this limit; in dimensional terms, this timescale ($\propto 1/\Omega_2$) is

$$\tau = \left[\frac{\nu\rho}{(\Delta\rho)_C}\right]^2 \frac{\alpha}{\kappa g}\frac{\mathrm{d}T}{\mathrm{d}z}.$$

Consequently there is no paradox of having an instability persist as the strength of the forcing goes to zero.

The basic flow of the single interface may be characterized as a viscous parallel jet influenced by buoyancy forces. Consequently, the stability of this flow has some similarities with the Kelvin–Helmholz problem. In particular the two problems have the property that the flow is unstable for a wide range of wavenumbers. One important difference is that the growth rate of the instability in the present problem is much longer than that in the Kelvin–Helmholz problem. The timescale for the growth of the instability in the Kelvin–Helmholz problem is (see Batchelor 1967, p. 516) L/U, where L is the width of the jet and U is the speed. In the present case, the growth rate is L/RU, where R is a small parameter, giving a much slower growth rate. This decrease in the rate of growth may be due to the action of the buoyancy forces parallel to the undisturbed interface.

5.3. *Mechanics of three-dimensional instability*

An unexpected feature of the instability found in the preceding sections is that, except for very small values of the Prandtl number, the most unstable mode has variation in the cross-flow direction, i.e. horizontally along the interface ($m \neq 0$). To understand this feature, we first note that the basic flow is driven by buoyancy differences created by thermal diffusion across the compositional interface, and retarded by viscosity. Consequently, as was noted in §4.3, the effects of thermal diffusion are nearly always destabilizing and those of viscosity are nearly always stabilizing.

As discussed in §3.4, the strength of the buoyancy flux is a measure of the vigour of the flow. The presence of cross-flow variation in the shape of the interface has the effect of increasing the buoyancy flux. To quantify this, consider the change buoyancy flux due to the zeroth-order neutral mode found in §4.1. To order R^0, $w^\dagger = \eta(y,z)f(x)$ and $T^\dagger = \eta(y,z)g(x)$ where $\eta = 2\epsilon\cos(my+nz)$,

$$f(x) = \sum_{j=1}^{3} \mu_j^3 A_j \exp(-\lambda_j|x|)$$

and

$$g(x) = \sum_{j=1}^{3} \mu_j^2 A_j \exp(-\lambda_j|x|).$$

The modified flux integrals are defined by

$$\tilde{F}_{\mathrm{H}} = \left\langle \int_{-\infty}^{\infty} (\bar{w}+w^\dagger)(\bar{T}+T^\dagger)\,\mathrm{d}x \right\rangle, \quad \tilde{F}_{\mathrm{m}} = \left\langle \int_{-\infty}^{\infty} (\bar{w}+w^\dagger)\bar{C}\,\mathrm{d}x \right\rangle,$$

where the angular brackets denote average over y and z. Noting that $\bar{w}$ and $\bar{T}$ are odd

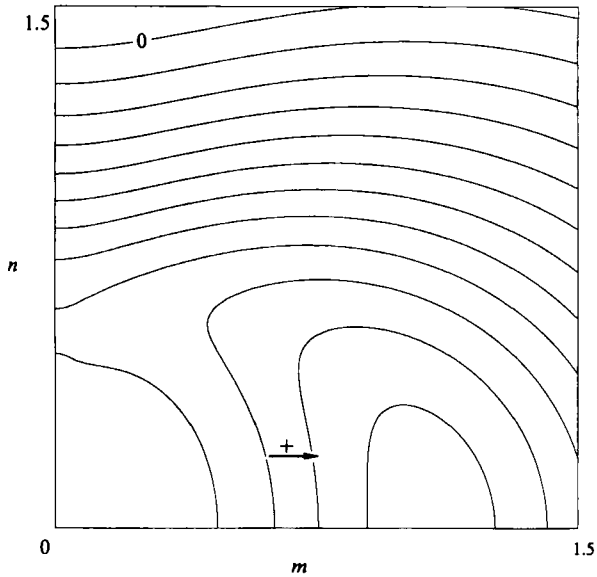

FIGURE 13. Isoline plot of the modified buoyancy flux, G, on the (m, n) wavenumber plane, taking into account the neutral deformation of the interface. This plot demonstrates that the flux is enhanced if the interface has variation in the cross-stream direction; i.e. if $m \neq 0$. The maximum value of G is 0.288; the contour interval is 0.025.

in x, f and g are (real and) even in x, and $\bar{C} = -\frac{1}{2}\operatorname{sgn}(x-\eta)$, these integrals may be expressed as

$$\tilde{F}_{\mathrm{H}} = \tilde{F}_{\mathrm{H0}} + \left\langle \eta^2 \int_{-\infty}^{\infty} fg \, \mathrm{d}x \right\rangle, \quad \tilde{F}_{\mathrm{m}} = \tilde{F}_{\mathrm{m0}} + \left\langle \int_0^{\eta} (\bar{w} + \eta f) \, \mathrm{d}x \right\rangle,$$

where a subscript 0 denotes the values for the undisplaced interface. Now $\bar{w} + \eta f \approx -(\frac{1}{4}x\sqrt{2}) + \eta f(0)$ for small x and $\langle \eta^2 \rangle = 2\epsilon^2$, so that

$$\tilde{F}_{\mathrm{H}} - \tilde{F}_{\mathrm{H0}} = 4\epsilon^2 \int_0^{\infty} fg \, \mathrm{d}x = 4\epsilon^2 \sum_{j=1}^{3} \sum_{k=1}^{3} \frac{\mu_j^3 \mu_k^2 A_j A_k}{\lambda_j + \lambda_k}$$

and

$$\tilde{F}_{\mathrm{m}} - \tilde{F}_{\mathrm{m0}} = 2\epsilon^2 \left[f(0) - \frac{1}{4\sqrt{2}} \right].$$

The buoyancy flux is the sum of these:

$$\tilde{F}_{\mathrm{B}} - \tilde{F}_{\mathrm{B0}} = \epsilon^2 G(m, n)$$

where

$$G(m, n) = \sum_{j=1}^{3} \mu_j^3 A_j \left[2 + 4 \sum_{k=1}^{3} \frac{\mu_k^2 A_k}{\lambda_j + \lambda_k} \right] - \frac{\sqrt{2}}{4}.$$

The isoline plot of G on the (m, n)-plane shown in figure 13 demonstrates that the buoyancy flux is enhanced if $m \neq 0$, and in fact reaches a maximum of 0.288 when $m = 1.07$ and $n = 0$.

5.4. *Effect of material diffusivity*

The analysis presented in the preceding sections is aimed at describing the stability of the cylindrical plumes shown emanating from chimneys in a porous matrix in figure 1. The problem of describing the flow within the matrix and chimneys has not yet been solved satisfactorily, in spite of several attempts (Roberts & Loper 1983;

Fowler 1985). Consequently, the compositional distribution within a plume as it leaves the crystal matrix is not known. We have modelled a uniform distribution with a sharp interface for all three configurations: single plane interface, two parallel interfaces and the cylindrical plume, with the hope that this will capture the essence of the stability even if the actual distribution is not uniform.

Material diffusion will act to broaden an initially sharp interface. Consequently the analysis of the preceding sections, which ignores material diffusivity, cannot be uniformly valid. Specifically, material diffusion limits the vertical extent of the interface; see Howard & Veronis (1987). This vertical extent can be estimated as follows.

The plume thickness, s_0, is determined by the salt-finger scale:

$$s_0 \approx (\nu\kappa/\alpha\gamma g)^{\frac{1}{4}}, \tag{5.1}$$

whereas the lateral extent, Δs, of the diffusing compositional interface is given by

$$\Delta s \approx (D\tau)^{\frac{1}{2}}, \tag{5.2}$$

where D is the material diffusivity and τ is the time the interface has been diffusing. The analysis of the preceding sections should remain valid provided

$$\Delta s \ll s_0. \tag{5.3}$$

The time τ may be thought of as a residence time, related to the vertical extent, h, of the plume and the velocity of rise, w, by

$$\tau \approx h/w. \tag{5.4}$$

The vertical velocity is scaled by

$$w \approx \beta\tilde{C}(g\kappa/\alpha\gamma\nu)^{\frac{1}{2}}. \tag{5.5}$$

Combining (5.1)–(5.5), we obtain a constraint on the vertical extent of the plume

$$h \ll \frac{\beta\tilde{C}}{\alpha\gamma}\frac{\kappa}{D}. \tag{5.6}$$

Noting that $\beta\tilde{C} = (\Delta\rho)_C/\rho_0$ and $\alpha\gamma h = (\Delta\rho)_T/\rho_0$, where $(\Delta\rho)_C$ is the density contrast induced by the compositional jump and $(\Delta\rho)_T$ is the density contrast induced by the vertical temperature contrast resulting from the imposed stable temperature gradient, (5.6) can be rewritten as

$$\frac{1}{R_\rho} = \frac{(\Delta\rho)_T}{(\Delta\rho)_C} \ll \frac{\kappa}{D}. \tag{5.7}$$

This is equivalent to condition (29) in Howard & Veronis (1987).

Commonly, thermal diffusivity is much larger than molecular compositional diffusivity so that the right-hand side of (5.7) is large. Also the compositionally induced density contrast is normally at least as large as the thermally induced contrast, particularly in the experiments depicted in figure 1. Therefore, condition (5.7) is often easily satisfied and material diffusivity may be ignored in studying the stability of isolated sharp interfaces.

This work was supported in part by grants EAR-8520678 and EAR-8805349 from the Earth Sciences Section of the National Science Foundation. This is publication no. 311 of the Geophysical Fluid Dynamics Institute, Florida State University, Tallahassee, Florida.

Appendix A. Jump conditions on the vertical velocity

The exact boundary conditions on the vertical velocity are that at $x = \eta$

$$\left.\begin{aligned} w(\eta-,y,z,t) &= w(\eta+,y,z,t), \\ \frac{\partial u}{\partial z}(\eta-,y,z,t)+\frac{\partial w}{\partial x}(\eta-,y,z,t) &= \frac{\partial u}{\partial z}(\eta+,y,z,t)+\frac{\partial w}{\partial x}(\eta+,y,z,t). \end{aligned}\right\} \tag{A 1}$$

The latter condition follows from continuity of stress. By Taylor expansion,

$$\left.\begin{aligned} w(\eta\pm;y,z,t) &= w(0\pm,y,z,t)+\eta\frac{\partial w}{\partial x}(0\pm,y,z,t)+\ldots, \\ \frac{\partial w}{\partial x}(\eta\pm,y,z,t) &= \frac{\partial w}{\partial x}(0\pm,y,z,t)+\eta\frac{\partial^2 w}{\partial x^2}(0\pm,y,z,t)+\ldots \end{aligned}\right\} \tag{A 2}$$

If we assume that

$$\left.\begin{aligned} w(x,y,z,t) &= \bar{w}(x)+\epsilon w^\dagger(x,y,z,t), \\ u(x,y,z,t) &= \mathrm{i}\epsilon u^\dagger(x,y,z,t) \end{aligned}\right\} \tag{A 3}$$

(A 2) becomes

$$\left.\begin{aligned} w(\eta\pm,y,z,t) &= \bar{w}(0\pm)+\epsilon w^\dagger(0\pm,y,z,t)+\eta\frac{\mathrm{d}\bar{w}}{\mathrm{d}x}(0\pm)+\ldots, \\ \frac{\partial w}{\partial x}(\eta\pm,y,z,t) &= \frac{\mathrm{d}\bar{w}}{\mathrm{d}x}(0\pm)+\epsilon\frac{\partial w^\dagger}{\partial x}(0\pm,y,z,t)+\eta\frac{\mathrm{d}^2\bar{w}}{\mathrm{d}x^2}(0\pm)+\ldots. \end{aligned}\right\} \tag{A 4}$$

We know that $\bar{w}$ and $\mathrm{d}\bar{w}/\mathrm{d}x$ are continuous at $x = 0$, so that the boundary conditions may be expressed as

$$\left.\begin{aligned} w^\dagger(0-) &= w^\dagger(0+), \\ \mathrm{i}\epsilon\frac{\partial u^\dagger}{\partial z}(0-)+\epsilon\frac{\partial w^\dagger}{\partial x}(0-) &= \mathrm{i}\epsilon\frac{\partial u^\dagger}{\partial z}(0+)+\epsilon\frac{\partial w^\dagger}{\partial x}(0+)+\eta\left[\frac{\mathrm{d}^2\bar{w}}{\mathrm{d}x^2}(0+)-\frac{\mathrm{d}^2\bar{w}}{\mathrm{d}x^2}(0-)\right]. \end{aligned}\right\} \tag{A 5}$$

Since the x-component of velocity is continuous at the interface, its derivative along the interface is also continuous: $\partial u^\dagger/\partial z(0-) = \partial u^\dagger/\partial z(0+)$.

Using standard pill-box arguments, the relevant terms of (2.20) are

$$\frac{\mathrm{d}^2\bar{w}}{\mathrm{d}x^2}+\bar{C} = 0.$$

From this it follows that

$$\frac{\mathrm{d}^2\bar{w}}{\mathrm{d}x^2}(0-)-\frac{\mathrm{d}^2\bar{w}}{\mathrm{d}x^2}(0+) = \bar{C}(0+)-\bar{C}(0-), \tag{A 6}$$

giving

$$w^\dagger(0-) = w^\dagger(0+), \quad \epsilon\frac{\mathrm{d}w^\dagger}{\mathrm{d}x}(0-) = \epsilon\frac{\mathrm{d}w^\dagger}{\mathrm{d}x}(0+)+\eta[\bar{C}(0-)-\bar{C}(0+)]. \tag{A 7}$$

For the single-line plume, $\bar{C}(0-)-\bar{C}(0+) = 1$. Assuming that η and $w^\dagger$ are given by (4.1) and (4.2), (A 7) yields (4.12*c*).

Appendix B. Solution of the single-plane-interface problem

In this appendix we shall derive the solution of (4.3), (4.5)–(4.7) and (4.13) subject to conditions (4.12). It is instructive to write the equations as

$$(\mathrm{d}^2/\mathrm{d}x^2-a^2)\,p-T=-2\mathrm{i}R(\bar{w})'u, \tag{B 1}$$

$$(\mathrm{d}^2/\mathrm{d}x^2-a^2)\,w+T+n^2p=\Omega w+\mathrm{i}nR\bar{w}w+\mathrm{i}R(\bar{w})'u, \tag{B 2}$$

$$(\mathrm{d}^2/\mathrm{d}x^2-a^2)\,T-w=\sigma\Omega T+\mathrm{i}\sigma R[n\bar{w}T+(\bar{T})'u], \tag{B 3}$$

$$(\mathrm{d}^2/\mathrm{d}x^2-a^2)\,v=-mnp+\Omega v+\mathrm{i}nR\bar{w}v, \tag{B 4}$$

$$\mathrm{d}u/\mathrm{d}x=-mv-nw. \tag{B 5}$$

B.1. *Zeroth-order problem*

Substitution of expansion (4.17) into this set of equations yields to dominant order a set with constant coefficients, so that we may replace $\mathrm{d}/\mathrm{d}x$ by $\lambda\,\mathrm{sgn}\,(x)$. To order R^0, (B 1)–(B 5) become

$$\left.\begin{aligned}\mu p_0-T_0=\mu w_0+T_0+n^2p_0=\mu T_0-w_0=0,\\ \mu v_0+mnp_0=\lambda\,\mathrm{sgn}\,(x)\,u_0+mv_0+nw_0=0,\end{aligned}\right\} \tag{B 6}$$

where

$$\mu=\lambda^2-a^2. \tag{B 7}$$

The appropriate boundary conditions are

$$\left.\begin{aligned}&w_0(0^-)=w_0(0^+),\quad T_0(0^-)=T_0(0^+),\quad \frac{\mathrm{d}w_0}{\mathrm{d}x}(0^-)=\frac{\mathrm{d}w_0}{\mathrm{d}x}(0^+)+1,\\ &\frac{\mathrm{d}T_0}{\mathrm{d}x}(0^-)=\frac{\mathrm{d}T_0}{\mathrm{d}x}(0^+),\quad p_0(0^-)=p_0(0^+),\quad v_0(0^-)=v_0(0^+),\\ &\frac{\mathrm{d}v_0}{\mathrm{d}x}(0^-)=\frac{\mathrm{d}v_0}{\mathrm{d}x}(0^+),\quad u_0(0^-)=u_0(0^+)=-\mathrm{i}\Omega_1.\end{aligned}\right\} \tag{B 8}$$

The dispersion relation for (B 6) is

$$\mu^3+\mu+n^2=0. \tag{B 9}$$

which is equivalent to (4.16). This yields three modes, λ_1, λ_2, and λ_3, with non-negative real part. It is easily verified that the solutions given by (4.18) satisfy (B 6) and (B 8).

Note that the functions u_0, v_0, w_0, T_0 and p_0 are all real. Further, u_0 is an odd function of x while the other variables are even in x.

B.2. *First-order problem*

To order R^1, (B 1)–(B 5) become (4.23)–(4.27). The forcing for this first-order problem comes from the non-homogeneous terms on the right-hand sides of (4.23)–(4.26); the boundary conditions are homogeneous at this order. Knowing that $\bar{w}$, $\bar{T}$, u_0, v_0, w_0 and T_0 are real, it follows that u_1, v_1, w_1, p_1 and T_1 are imaginary. Also with $\bar{w}$, $\bar{T}$ and u_0 odd and v_0, p_0, w_0 and T_0 even in x, it follows that u_1 is even and v_1, w_1, p_1 and T_1 are odd in x. We shall use this symmetry property to simplify the following solution.

The general solution of this set of equations may be expressed as the sum of homogeneous and particular solutions:

$$w_1=w_\mathrm{h}+w_\mathrm{p},\quad \text{etc.} \tag{B 10}$$

The homogeneous solutions are functionally identical to (4.18), but with differing complex character; let

$$\{w_{\mathrm{h}}^{\pm}, p_{\mathrm{h}}^{\pm}, T_{\mathrm{h}}^{\pm}\} = \pm \sum_{j=1}^{3} \{\mu_j^3, \mu_j, \mu_j^2\} \mathrm{i} B_j \exp(-\lambda_j |x|), \tag{B 11}$$

where superscripts + and − denote solutions valid for $0<x$ and $0>x$, respectively.

In the present notation, (3.5) and (3.6) are

$$\bar{w}^{\pm} = \pm \tfrac{1}{2} \mathrm{Im}\,[\exp(-k|x|)], \tag{B 12}$$

and

$$\bar{T}^{\pm} = \pm \tfrac{1}{2} \mathrm{Im}\,[\mathrm{i} - \mathrm{i} \exp(-k|x|)]. \tag{B 13}$$

Noting that u_0, v_0, w_0 and T_0 are real, (4.23)–(4.25) may be expressed as

$$\left(\frac{\mathrm{d}^2}{\mathrm{d}x^2} - a^2\right) p_{\mathrm{p}} - T_{\mathrm{p}} = \pm \tfrac{1}{2} \mathrm{i} n \,\mathrm{Im}\left[\sum_{j=1}^{3} -2k\lambda_j A_j \exp[-(\lambda_j + k)|x|]\right], \tag{B 14}$$

$$\left(\frac{\mathrm{d}^2}{\mathrm{d}x^2} - a^2\right) w_{\mathrm{p}} + T_{\mathrm{p}} + n^2 p_{\mathrm{p}} = \pm \tfrac{1}{2} \mathrm{i} n \,\mathrm{Im}\left[\sum_{j=1}^{3} A_j(\mu_j^3 + k\lambda_j) \exp[-(\lambda_j + k)|x|]\right], \tag{B 15}$$

$$\left(\frac{\mathrm{d}^2}{\mathrm{d}x^2} - a^2\right) T_{\mathrm{p}} - w_{\mathrm{p}} = \pm \tfrac{1}{2} \mathrm{i} n \sigma \,\mathrm{Im}\left[\sum_{j=1}^{3} A_j(\mu_j^2 - \mathrm{i}k\lambda_j) \exp[-(\lambda_j + k)|x|]\right]. \tag{B 16}$$

Defining

$$\{w_{\mathrm{p}}^{\pm}, p_{\mathrm{p}}^{\pm}, T_{\mathrm{p}}^{\pm}\} = \pm \tfrac{1}{2} \mathrm{i} n \,\mathrm{Im}\left[\sum_{j=1}^{3} A_j \{w_j, p_j, T_j\} \exp[-(\lambda_j + k)|x|]\right], \tag{B 17}$$

the particular solutions of (B 14)–(B 16) must satisfy

$$\left.\begin{aligned} \gamma_j p_j - T_j &= -2k\lambda_j, \\ \gamma_j w_j + n^2 p_j + T_j &= (\mu_j)^3 + k\lambda_j, \\ -w_j \qquad + \gamma_j T_j &= \sigma[(\mu_j)^2 - \mathrm{i}k\lambda_j], \end{aligned}\right\} \tag{B 18}$$

where γ_j is defined by (4.37). Note that the variables w_j, p_j, and T_j defined by (B 17) are different from w_α, p_α, and T_α introduced by (4.17).

The solution of (B 18) may be expressed as

$$\left.\begin{aligned} w_j &= \frac{1}{D_j}[n^2\gamma_j 2k\lambda_j + \gamma_j^2(\mu_j^3 + k\lambda_j) - (\gamma_j + n^2)\sigma(\mu_j^2 - \mathrm{i}k\lambda_j)], \\ p_j &= \frac{1}{D_j}[-(1+\gamma_j^2) 2k\lambda_j + (\mu_j^3 + k\lambda_j) + \gamma_j \sigma(\mu_j^2 - \mathrm{i}k\lambda_j)], \\ T_j &= \frac{1}{D_j}[n^2 2k\lambda_j + \gamma_j(\mu_j^3 + k\lambda_j) + \gamma_j^2 \sigma(\mu_j^2 - \mathrm{i}k\lambda_j)], \end{aligned}\right\} \tag{B 19}$$

where D_j is given by (4.37). The variables $w_{\mathrm{I}}^{\pm}$, $p_{\mathrm{I}}^{\pm}$ and $T_{\mathrm{I}}^{\pm}$ must satisfy the continuity conditions (4.28).

Using (4.18), (B 11), (B 12) and (B 17), (4.26) may be expressed as

$$\left(\frac{\mathrm{d}^2}{\mathrm{d}x^2} - a^2\right) v_{\mathrm{I}} = -\mathrm{i}mn \sum_{j=1}^{3} \mu_j B_j \exp[-\lambda_j |x|] \pm \tfrac{1}{2} \mathrm{i} m n^2 \,\mathrm{Im}\left[\sum_{j=1}^{3} A_j(-p_j - 1) \exp[-(\lambda_j + k)|x|]\right]. \tag{B 20}$$

The general solution of this equation satisfying the symmetry conditions is

$$v_1^{\pm} = \pm \mathrm{i}aB_4 \exp(-a|x|) \mp imn \sum_{j=1}^{3} B_j \exp(-\lambda_j|x|) \pm \tfrac{1}{2}in \operatorname{Im}\left\{\sum_{j=1}^{3} A_j v_j \exp[-(\lambda_j+k)|x|]\right\}, \quad \text{(B 21)}$$

where

$$v_j = -mn\frac{(p_j+1)}{\gamma_j}. \quad \text{(B 22)}$$

With v_1 and w_1 given by (B 21), (B 11) and (B 17), the solution of (4.27) is

$$u_1^{\pm} = imB_4 \exp(-a|x|) - in \sum_{j=1}^{3} B_j \lambda_j \exp(-\lambda_j|x|) + \tfrac{1}{2}in \operatorname{Im}\left\{\sum_{j=1}^{3} A_j u_j \exp[-(\lambda_j+k)|x|]\right\}, \quad \text{(B 23)}$$

where

$$u_j = \frac{[mv_j + nw_j]}{\lambda_j + k}. \quad \text{(B 24)}$$

These solutions must satisfy conditions (4.29).

Conditions (4.28) and (4.29) are satisfied provided

$$\sum_{j=1}^{3} \{\mu_j^3, \mu_j, \mu_j^2\} B_j = \{\hat{w}, \hat{p}, \hat{T}\}, \quad \text{(B 25)}$$

$$aB_4 - mn \sum_{j=1}^{3} B_j = \hat{v}, \quad \Omega_2 = -mB_4 + n \sum_{j=1}^{3} \lambda_j B_j + \hat{u}, \quad \text{(B 26), (B 27)}$$

where

$$\hat{y} = -\tfrac{1}{2}n \operatorname{Im}\left[\sum_{j=1}^{3} A_j y_j\right] \quad \text{(B 28)}$$

for $y = w, p, T, u$, and v. Condition (B 27) serves to determine Ω_2 once the coefficients B_j and B_4 are determined.

Using (B 9) and noting that

$$\sum_{j=1}^{3} \frac{\{\mu_j^{-1}, 1, \mu_j, \mu_j^2, \mu_j^3, \mu_j^4, \mu_j^5\}}{3n^2 + 2\mu_j} = \{-n^{-4}, n^{-2}, 0, 0, -1, 0, 1\}, \quad \text{(B 29)}$$

these may be expressed as

$$B_j = -\frac{[\mu_j^2 \hat{T} + \mu_j \hat{w} - n^2 \hat{p}]}{\mu_j[3n^2 + 2\mu_j]}. \quad \text{(B 30)}$$

Also noting that

$$\sum_{j=1}^{3} B_j = -\frac{(\hat{w}+\hat{p})}{n^2}, \quad \text{(B 31)}$$

(B 26) yields

$$B_4 = \frac{\hat{v}}{a} - \frac{m}{an}(\hat{w}+\hat{p}). \quad \text{(B 32)}$$

Making use of the fact that any expression of the form

$$\sum_{j=1}^{3} f(\mu_j, \lambda_j, A_j)$$

is purely real, the dispersion relation (B 27) may be expressed as (4.30). Note that Ω_2 is purely real.

REFERENCES

ABRAMOWITZ, M. & STEGUN, I. A. 1965 *Handbook of Mathematical Functions*. Dover.

BATCHELOR, G. K. 1967 *An Introduction to Fluid Dynamics*. Cambridge University Press.

CHAPMAN, D. C. 1986 A simple model of the formation and maintenance of the shelf-slope front in the middle Atlantic bight. *J. Phys. Oceanogr.* **16**, 1273–1279.

CHEN, C. F. & JOHNSON, D. H. 1984 Double-diffusive convection: a report on an engineering foundation conference. *J. Fluid Mech.* **138**, 405–416.

COPLEY, S. M., GIAMI, A. F., JOHNSON, S. M. & HORNBECKER, M. F. 1970 On the origin of freckles in unidirectionally solidified castings. *Metall. Trans.* **1**, 2193–2204.

DRAZIN, P. G. & REID, W. H. 1981 *Hydrodynamic Instability*. Cambridge University Press.

DUDIS, J. J. & DAVIS, S. H. 1971 Energy stability of the buoyancy boundary layer. *J. Fluid Mech.* **47**, 381–403.

ELTAYEB, I. A. 1972 Hydromagnetic convection in a rapidly rotating layer. *Proc. R. Soc. Lond.* A **326**, 229–254.

FOWLER, A. C. 1985 The formation of freckles in binary alloys. *IMA J. Appl. Maths* **35**, 159–174.

GILL, A. E. 1966 The boundary-layer regime for convection in a rectangular cavity. *J. Fluid Mech.* **26**, 515–536.

GILL, A. E. & DAVEY, A. 1969 Instabilities of a buoyancy-driven system. *J. Fluid Mech.* **35**, 775–798.

HOLYER, J. Y. 1983 Double diffusive interleaving due to horizontal gradients. *J. Fluid Mech.* **137**, 347–362.

HOWARD, L. N. & VERONIS, G. 1987 The salt-finger zone. *J. Fluid Mech.* **183**, 1–23 (referred to herein as H&V).

HSUEH, Y. & CUSHMAN-ROISIN, B. 1983 On the formation of surface to bottom fronts over steep topography. *J. Geophys. Res.* **88**, 743–750.

HUPPERT, H. E. & MOORE, D. R. 1976 Nonlinear double diffusive convection. *J. Fluid Mech.* **78**, 821–854.

LOPER, D. E. 1989 Dynamo energetics and the structure of the outer core. *Geophys. Astrophys. Fluid Dyn.* **49**, 213–219.

OU, H. W. 1983 Some two-layer models of the shelf-slope front: geostrophic adjustment and its maintenance. *J. Phys. Oceanogr.* **13**, 1798–1808.

ROBERTS, P. H. & LOPER, D. E. 1983 Towards a theory of the structure and evolution of a dendrite layer. In *Stellar and Planetary Magnetism* (ed. A. M. Soward), pp. 329–349. Gordon and Breach.

TURNER, J. S. 1973 *Buoyancy Effects in Fluids*. Cambridge University Press.

TURNER, J. S. 1985 Multicomponent convection. *Ann. Rev. Fluid Mech.* **17**, 11–44.

WANG, D.-P. 1984 Mutual intrusion of a gravity current and density front formation. *J. Phys. Oceanogr.* **14**, 1191–1199.